

Simple Distances for Trajectories via Landmarks

Jeff M. Phillips
jeffp@cs.utah.edu

School of Computing, University of Utah.
Salt Lake City, Utah, USA

Pingfan Tang

tang1984@cs.utah.edu

School of Computing, University of Utah.
Salt Lake City, Utah, USA

Abstract

We develop a new class of distances for objects including lines, hyperplanes, and trajectories, based on the distance to a set of landmarks. These distances easily and interpretably map objects to a Euclidean space, are simple to compute, and perform well in data analysis tasks. For trajectories, they match and in some cases significantly out-perform all state-of-the-art other metrics, can effortlessly be used in k -means clustering, and directly plugged into approximate nearest neighbor approaches which immediately out-perform the best recent advances in trajectory similarity search by several orders of magnitude. These distances do not require a geometry distorting dual (common in the line or halfspace case) or complicated alignment (common in trajectory case). We show reasonable and often simple conditions under which these distances are metrics.

CCS Concepts

• **Computing methodologies** → **Feature selection**; • **Theory of computation** → *Randomness, geometry and discrete structures*;

Keywords

trajectory similarity, trajectory classification, sketching

ACM Reference Format:

Jeff M. Phillips and Pingfan Tang . 2019. Simple Distances for Trajectories via Landmarks.

1 Introduction

The *choice* of a distance is often the most important modeling decision in any data analysis task. This choice is what determines which objects are close and which are far. However, this task is often taken lightly or made just based on what provides the simplest or easiest to compute option.

In this paper we explore what we believe to be a new and natural family of distances between objects, focusing on two cases when the objects are hyperplanes (e.g., regressors or separators), or when they are trajectories. Our proposed distance d_Q uses a set Q of

landmark points, which could be the dataset that regressors or separators are trained on, or in the case of trajectories these may be points of interest for which a trajectory passing nearby has specific meaning. However, in a general case, Q can be chosen as arbitrary or random points placed to cover a domain of focus. Then the new distances, instead of being directly between the objects themselves, are based on how they interact with the set of landmarks. In the simplest variant, for n landmarks Q , for any object J we create an n -dimensional vector $v_J = (v_1, v_2, \dots, v_n)$ of the distance from $q_i \in Q$ to J , and the distance between two objects J_1 and J_2 is the Euclidean distance between the vectors $\|v_{J_1} - v_{J_2}\|$. In other words, we *vectorize* the distance between complex objects.

In this paper we explore several variants of this formulation, derive convenient mathematical properties, and demonstrate its efficacy in several data analysis scenarios.

Key properties of a distance. A definition of a distance d is the key building block in most data analysis tasks. For instance, it is at the heart of any assignment-based clustering (e.g., k -means) or for nearest-neighbor searching and analysis. We can also define a radial-basis kernel $K(p, q) = \exp(-d(p, q)^2)$ (or similarly), which is required for kernel SVM classification, kernel regression, and kernel density estimation. A change in the distance, directly affects the meaning and modeling inherent in each of these tasks. So the first consideration in choosing a distance should always be, does it capture the properties between the objects that matter?

As we will observe, by having a distance depend on a set of landmarks Q , then we can tune it to focus on certain regions. In the case of regressors or separators (e.g., infinite lines, hyperplanes) this makes sure the distance is determined by how these infinite objects interact with the support of the data. In the case of trajectories, the distance can be adjusted to focus on one or more locations of interest (e.g., a sporting event or school) or regions of interest (e.g., how someone passes through an airport, but not how they get there), as opposed to its full geometry.

A generic desired property of a distance is that it should be a metric: for instance this is essential in the analysis for the Gonzalez algorithm [11] for k -center clustering, and many other contexts such as nearest-neighbor searching.

Another generic goal is analyzing the distance's metric balls. That is, given a set of objects \mathcal{J} and a distance $d : \mathcal{J} \times \mathcal{J} \rightarrow \mathbb{R}$, let $B(J, r) = \{J' \in \mathcal{J} \mid d(J, J') \leq r\}$ be a metric ball around $J \in \mathcal{J}$ of radius r . Then we can define a range space $(\mathcal{J}, \mathcal{R})$ where $\mathcal{R} = \{B(J, r) \mid J \in \mathcal{J}, r \geq 0\}$, and consider its VC-dimension [20]. When the VC-dimension v is small, it implies that the metric balls cannot interact with each other in a too complex way, indicating the distance is roughly as well-behaved as a v -dimensional Euclidean ball. More directly, this implies, decision boundaries to classify objects can be learned with only ε -fraction generalization error using $O(v/\varepsilon \cdot \log(1/\varepsilon))$ samples if the data is separable, or $O(v/\varepsilon^2)$ samples

Permission to make digital or hard copies of part or all of this work for personal or classroom use is granted without fee provided that copies are not made or distributed for profit or commercial advantage and that copies bear this notice and the full citation on the first page. Copyrights for third-party components of this work must be honored. For all other uses, contact the owner/author(s).

Jeff Phillips thanks his support from NSF CCF-1350888, ACI-1443046, CNS- 1514520, CNS-1564287, and IIS-1816149. Part of the work was completed while visiting the Simons Institute for Theory of Computing.

© 2019 Copyright held by the owner/author(s).

if the data is not separable [14]. Similar bounds can be shown for other tasks such as preserving kernel density estimates derived from such distances [13]. In other words, this ensures that many tasks are stable with respect to the underlying family of objects \mathcal{J} .

Main results. We define a new data dependent distance d_Q for trajectories and for linear models (e.g., regressors, separators) built from a landmark data set Q . For the simpler cases of linear models (in Section 2), we show it is a metric as long as Q is full rank. We also show that its metric balls have VC-dimension bounded only by the ambient dimension and not on the size of Q . We find this surprising because the distance corresponds to an embedding in $|Q|$ -dimensional Euclidean space where an immediate bound for the VC-dimension is $|Q| + 1$; and indeed this will be the best bound we have for most of the trajectory variants. We show how to directly extend all of these definitions of lines to trajectories, with a somewhat unintuitive and restrictive distance measure d_Q^{\leftrightarrow} .

For the pressing scenario of trajectories, in Section 3, we introduce two more intuitive variants d_Q and d_Q^π . We describe simple conditions for Q under which they are metrics. We can immediately see that both distances are pseudometrics (they satisfy triangle inequality, and are symmetric, but might have distinct objects with distance 0). We show they satisfy the final 0-property of a metric as long as the waypoints are distinct and Q is sufficiently dense. For all new variants we demonstrate that they are at the least as effective for classification tasks (via KNN classifiers) as compared to the best of 9 other common metrics, and *in some cases significantly outperforms all of these measures*. Moreover, the previous competing variants are typically significantly more complicated or computationally intensive, and may require parameter tuning.

In contrast to most of these trajectory distance alternatives, all of our proposed distances are very simple to compute and work with. They map curves (or hyperplanes) to a $|Q|$ -dimensional parameter space where Euclidean distance (or similar) is used. In d_Q for curves, each coordinate v_i is the distance to the closest point on the curve from $q_i \in Q$. In d_Q^π each “coordinate” is actually the d coordinates of the closest point on the curve (not just the distance). In d_Q^{\leftrightarrow} each “coordinate” v_i is actually k values, to the distance to the closest point on the k lines extending the k line segments of the curve. These mappings are effective with only 10 or 20 landmark points Q . And because they have a familiar Euclidean structure, we can immediately invoke favorite algorithms in this space, from Lloyds for k -means clustering, linear and kernel SVM, and highly-engineered approximate nearest neighbor libraries. In comparison to recent trajectory similarity search systems [19, 23], we show using d_Q is much simpler and several orders of magnitude faster.

In summary, this paper introduces a family of metrics for regressors, separators, and piecewise-linear curves which are incredibly simple to use, provide a sketch vector in Euclidean space, have many other desirable mathematical properties, and perform as well as and often significantly better than any existing measure.

2 Distance Between Lines and Hyperplanes

As a warm up to the general case, we define a new landmark-based distance d_Q between two lines, and give the condition under which it is a metric. Then we generalize to hyperplanes, and provide the

general metric proof, the VC-dimension of metric ball proof, and some algorithmic implications. We conclude with a direct extension to trajectories.

2.1 Warm Up: Distance Between Lines

We begin by reviewing alternatives, starting with the default *dual Euclidean distance*. Consider the least square regression problem in \mathbb{R}^2 : given $Q = \{(x_1, y_1), \dots, (x_n, y_n)\} \subset \mathbb{R}^2$, return a line $\ell : y = ax + b$ such that $(a, b) = \arg \min_{(a,b) \in \mathbb{R}^2} \sum_{i=1}^n (ax_i + b - y_i)^2$. If $\ell_1 : y = a_1x + b_1$ is an alternate fit to this data, then to measure the difference in these variants, we can define a distance between ℓ and ℓ_1 . A simple and commonly used distance (which we called the *dual-Euclidean distance*) is

$$d_{dE}(\ell, \ell_1) := \sqrt{(a - a_1)^2 + (b - b_1)^2}.$$

This can be viewed as dualizing the lines into a space defined by their parameters (slope a and intercept b), and then taking the Euclidean distance between these parametric points. However, as shown in Figure 1(Left), if both ℓ_1 and ℓ_2 have the same slope $a_1 = a_2$, and are offset the same amount from ℓ ($|b - b_1| = |b - b_2|$), then $d_{dE}(\ell, \ell_1) = d_{dE}(\ell, \ell_2)$, although intuitively ℓ_1 does a much more similar job to ℓ with respect to Q than does ℓ_2 .

More generically, a geometric object is usually described by an (often compact) set in \mathbb{R}^d . There are many ways to define and compute distances between such objects [1, 2, 9, 10]. These can be based on the minimum [9, 10] or maximum (e.g., Hausdorff) [1, 2] distance between objects. We review more later in the context of trajectories in Section 4.1. For lines or hyperplanes which extend infinitely and may intersect at single points, such measures are not meaningful.

Our formulation. Suppose $Q = \{q_1, q_2, \dots, q_n\} \subset \mathbb{R}^2$ where q_i has coordinates (x_i, y_i) for $1 \leq i \leq n$, and ℓ is a line in \mathbb{R}^2 , then ℓ can be uniquely expressed as

$$\ell = \{(x, y) \in \mathbb{R}^2 \mid u_1x + u_2y + u_3 = 0\},$$

where $(u_1, u_2, u_3) \in \mathbb{U}^3$. Here $\mathbb{U}^3 = \{u = (u_1, u_2, u_3) \in \mathbb{R}^3 \mid u_1^2 + u_2^2 = 1 \text{ and the first nonzero entry of } u \text{ is positive}\}$, is a canonical way to normalize u where (u_1, u_2) is unit normal vector and u_3 is an offset parameter. Let $v_{Q_i}(\ell) = u_1x_i + u_2y_i + u_3$; it is the signed distance from $q_i = (x_i, y_i)$ to the closest point on ℓ . Then

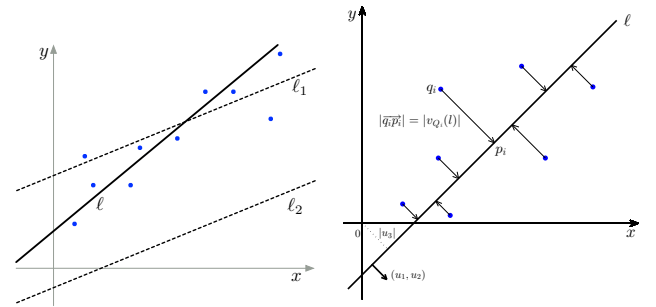


Figure 1: Left: $d_{dE}(\ell, \ell_1) = d_{dE}(\ell, \ell_2)$, but which of ℓ_1 and ℓ_2 is more similar to ℓ with respect to Q ? **Right:** Each p_i is the projection of q_i on ℓ .

$v_Q(\ell) = (v_{Q_1}(\ell), v_{Q_2}(\ell), \dots, v_{Q_n}(\ell))$ is the n -dimensional vector of these distances. For two lines ℓ_1, ℓ_2 in \mathbb{R}^2 , we can now define

$$\begin{aligned} d_Q(\ell_1, \ell_2) &= \left\| \frac{1}{\sqrt{n}}(v_Q(\ell_1) - v_Q(\ell_2)) \right\| \\ &= \left(\sum_{i=1}^n \frac{1}{n} (v_{Q_i}(\ell_1) - v_{Q_i}(\ell_2))^2 \right)^{\frac{1}{2}}. \end{aligned}$$

As shown in Figure 1(Right), $|v_{Q_i}(\ell)|$ is the distance from q_i to ℓ . With the help of Q , we convert each line ℓ in \mathbb{R}^2 to point $\frac{1}{\sqrt{n}}v_Q(\ell)$ in \mathbb{R}^n , and use the Euclidean distance between two points to define the distance between the original two lines. Via this Euclidean embedding, it directly follows that d_Q is symmetric and follows the triangle inequality. The following theorem shows, under reasonable assumptions of Q , no two different lines can be mapped to the same point in \mathbb{R}^n , so d_Q is a metric.

THEOREM 2.1. *Suppose in $Q = \{(x_1, y_1), (x_2, y_2), \dots, (x_n, y_n)\} \subset \mathbb{R}^2$ there are three non-collinear points, and $\mathcal{L} = \{\ell \mid \ell \text{ is a line in } \mathbb{R}^2\}$, then d_Q is a metric in \mathcal{L} .*

PROOF. The function $d_Q(\cdot, \cdot)$ is symmetric and by mapping to \mathbb{R}^n satisfies the triangle inequality, and $\ell_1 = \ell_2$ implies $d_Q(\ell_1, \ell_2) = 0$; we now show if $d_Q(\ell_1, \ell_2) = 0$, then $\ell_1 = \ell_2$.

Without loss of generality, we assume $(x_1, y_1), (x_2, y_2), (x_3, y_3) \in Q$ are not on the same line, which implies

$$\begin{vmatrix} x_1 & y_1 & 1 \\ x_2 & y_2 & 1 \\ x_3 & y_3 & 1 \end{vmatrix} \neq 0. \quad (1)$$

Suppose ℓ_1 and ℓ_2 are expressed in the form:

$$\begin{aligned} \ell_1 &= \{(x, y) \in \mathbb{R} \mid u_1^{(1)}x + u_2^{(1)}y + u_3^{(1)} = 0\}, \\ \ell_2 &= \{(x, y) \in \mathbb{R} \mid u_1^{(2)}x + u_2^{(2)}y + u_3^{(2)} = 0\}, \end{aligned}$$

where $(u_1^{(1)}, u_2^{(1)}, u_3^{(1)}), (u_1^{(2)}, u_2^{(2)}, u_3^{(2)}) \in \mathbb{U}^3$ represent lines ℓ_1 and ℓ_2 , respectively. If $d_Q(\ell_1, \ell_2) = 0$, then we have

$$x_i(u_1^{(1)} - u_1^{(2)}) + y_i(u_2^{(1)} - u_2^{(2)}) + (u_3^{(1)} - u_3^{(2)}) = 0$$

for $i = 1, 2, 3$. We can write this as the system

$$\begin{bmatrix} x_1 & y_1 & 1 \\ x_2 & y_2 & 1 \\ x_3 & y_3 & 1 \end{bmatrix} \begin{bmatrix} u_1^{(1)} - u_1^{(2)} \\ u_2^{(1)} - u_2^{(2)} \\ u_3^{(1)} - u_3^{(2)} \end{bmatrix} = 0.$$

Using (1), we know it has the unique solution $[u_1^{(1)} - u_1^{(2)}, u_2^{(1)} - u_2^{(2)}, u_3^{(1)} - u_3^{(2)}]^T = [0, 0, 0]^T$. So, we have $u_1^{(1)} = u_1^{(2)}$, $u_2^{(1)} = u_2^{(2)}$ and $u_3^{(1)} = u_3^{(2)}$, and thus $\ell_1 = \ell_2$. \square

Remark. In the above formulation, the absolute value $|v_{Q_i}(\ell)|$ is the distance from (x_i, y_i) to the line ℓ , i.e. $|v_{Q_i}(\ell)| = \min_{(x, y) \in \ell} ((x - x_i)^2 + (y - y_i)^2)^{\frac{1}{2}}$. Moreover, if ℓ is parallel to ℓ' , then $|v_{Q_i}(\ell) - v_{Q_i}(\ell')| = \min_{(x, y) \in \ell, (x', y') \in \ell'} ((x - x')^2 + (y - y')^2)^{\frac{1}{2}}$ for any $i \in [n]$, which means d_Q is a generalization of the natural offset distance between two parallel lines.

Remark. There are several other nicely defined variants of this distance. For a line ℓ we could define $\bar{v}_{Q_i}(\ell) = |v_{Q_i}(\ell)|$, as the *unsigned* distance from $q_i \in Q$ to the line ℓ . When we consider the distance from q_i to some bounded object (e.g., a trajectory in place of ℓ), this distance is more natural. We are able to show in Appendix A that under similar mild restrictions on Q that this is a metric; the condition requires 5 points instead of 3. However, we are not able to show constant-size VC-dimension for its metric balls (as we do for d_Q in Section 2.3). There we also introduce another matrix Frobenius norm variant.

2.2 Distance Between Hyperplanes

Now let $\mathcal{H} = \{h \mid h \text{ is a hyperplane in } \mathbb{R}^d\}$ represent the space of all hyperplanes. Suppose $Q = \{q_1, q_2, \dots, q_n\} \subset \mathbb{R}^d$, where q_i has the coordinate $(x_{i,1}, x_{i,2}, \dots, x_{i,d})$. Any hyperplane $h \in \mathcal{H}$ can be uniquely expressed in the form

$$h = \{x = (x_1, \dots, x_d) \in \mathbb{R}^d \mid \sum_{j=1}^d u_j x_j + u_{d+1} = 0\},$$

where (u_1, \dots, u_{d+1}) is a vector in $\mathbb{U}^{d+1} := \{u = (u_1, \dots, u_{d+1}) \in \mathbb{R}^{d+1} \mid \sum_{j=1}^d u_j^2 = 1 \text{ and the first nonzero entry of } u \text{ is positive}\}$, i.e. (u_1, \dots, u_d) is the unit normal vector of h , and u_{d+1} is the offset. We introduce the notation $v_Q(h) = (v_{Q_1}(h), \dots, v_{Q_n}(h))$ where $v_{Q_i}(h)$ is again the signed distance from q_i to the closest point on h . We can specify $v_{Q_i}(h) = \sum_{j=1}^d u_j x_{i,j} + u_{d+1}$, which is a dot-product with the unit normal of h , plus offset u_{d+1} . Now for two hyperplanes h_1, h_2 in \mathbb{R}^d define

$$\begin{aligned} d_Q(h_1, h_2) &:= \left\| \frac{1}{\sqrt{n}}(v_Q(h_1) - v_Q(h_2)) \right\| \\ &= \left(\sum_{i=1}^n \frac{1}{n} (v_{Q_i}(h_1) - v_{Q_i}(h_2))^2 \right)^{\frac{1}{2}}. \end{aligned}$$

For $Q \subset \mathbb{R}^d$, similar to d_Q in \mathbb{R}^2 , we want to consider the case that there are $d+1$ points in Q which are not on the same hyperplane. We refer to such a point set Q as *full rank* since if we treat the points as rows, and stack them to form a matrix, then that matrix is full rank. Like lines in \mathbb{R}^2 , a hyperplane can also be mapped to a point in \mathbb{R}^n , and if Q is full rank, then no two hyperplanes will be mapped to the same point in \mathbb{R}^n . So, similar to Theorem 2.1, we can prove d_Q is a metric in \mathcal{H} .

THEOREM 2.2. *If $Q = \{q_1, q_2, \dots, q_n\} \subset \mathbb{R}^d$ is full rank, then d_Q is a metric in \mathcal{H} .*

Remark. The distance can be generalized to weighted point sets and continuous probability distributions. Suppose $Q = \{q_1, \dots, q_n\} \subset \mathbb{R}^d$, $W = \{w_1, \dots, w_n\} \subset (0, \infty)$, and μ is a probability measure on \mathbb{R}^d . For two hyperplanes h_1, h_2 in \mathbb{R}^d , we define

$$\begin{aligned} d_{Q,W}(h_1, h_2) &= \left(\sum_{i=1}^n w_i (v_{Q_i}(h_1) - v_{Q_i}(h_2))^2 \right)^{\frac{1}{2}}, \\ d_\mu(h_1, h_2) &= \left(\int_{\mathbb{R}^d} (v_x(h_1) - v_x(h_2))^2 d\mu(x) \right)^{\frac{1}{2}}, \end{aligned}$$

where $v_x(\cdot)$ is defined in the same way as $v_{Q_i}(\cdot)$ for $x \in \mathbb{R}^d$.

2.3 VC-Dimension of Metric Balls for d_Q

The distance d_Q can induce a range space $(\mathcal{H}, \mathcal{R}_Q)$, where again \mathcal{H} is the collection of all hyperplanes in \mathbb{R}^d , and $\mathcal{R}_Q = \{B_Q(h, r) \mid h \in \mathcal{H}, r \geq 0\}$ with metric ball $B_Q(h, r) = \{h' \in \mathcal{H} \mid d_Q(h, h') \leq r\}$. We prove that the VC dimension [20] of this range space only depends on d , and is independent of the number of points in Q .

THEOREM 2.3. *Suppose $Q \subset \mathbb{R}^d$ is full rank, then the VC-dimension of the range space $(\mathcal{H}, \mathcal{R}_Q)$ is at most $\frac{1}{2}(d^2 + 5d + 6)$.*

PROOF. For any $B_Q(h_0, r) \in \mathcal{R}_Q$, suppose $Q = \{x_1, \dots, x_n\}$ with $x_i = (x_{i,1}, \dots, x_{i,d})$ and $h \in B_Q(h_0, r)$. This implies $d_Q(h, h_0) \leq r$, so if h is represented by a unique vector $(u_1, \dots, u_{d+1}) \in \mathbb{U}^{d+1}$, then we have

$$\sum_{i=1}^n \frac{1}{n} \left(\sum_{j=1}^d u_j x_{i,j} + u_{d+1} - v_{Q_i}(h_0) \right)^2 \leq r^2. \quad (2)$$

Since this can be viewed as a polynomial of u_1, \dots, u_{d+1} , we can use a standard lifting map to convert it to a linear equation about new variables, and then use the VC-dimension of the collection of halfspaces to prove the result.

To this end, we introduce the following data parameters a_j [for $0 \leq j \leq d+1$] and $a_{j,j'}$ [for $1 \leq j \leq j' \leq d+1$] which only depend on Q , h_0 , and r . That is these only depend on the metric d_Q and the choice of metric ball.

$$\begin{aligned} a_0 &= \sum_{i=1}^n v_{Q_i}(h_0)^2 - nr^2, & a_{d+1} &= -2 \sum_{i=1}^n v_{Q_i}(h_0), \\ a_j &= -2 \sum_{i=1}^n x_{i,j} v_{Q_i}(h_0) \text{ [for } 1 \leq j \leq d], \\ a_{d+1, d+1} &= n, & a_{j, d+1} &= 2 \sum_{i=1}^n x_{i,j} \text{ [for } 1 \leq j \leq d], \\ a_{j,j} &= \sum_{i=1}^n x_{i,j}^2 \text{ [for } 1 \leq j \leq d], & \text{and} \\ a_{j,j'} &= 2 \sum_{i=1}^n x_{i,j} x_{i,j'} \text{ [for } 1 \leq j < j' \leq d]. \end{aligned}$$

We also introduce another set of new variables y_j [for $1 \leq j \leq d+1$] and $y_{j,j'}$ [for $1 \leq j \leq j' \leq d+1$] which only depend on the choice of h :

$$\begin{aligned} y_j &= u_j \text{ [for } 1 \leq j \leq d+1] \quad \text{and} \\ y_{j,j'} &= u_j u_{j'} \text{ [for } 1 \leq j \leq j' \leq d+1]. \end{aligned}$$

Now (2) can be further rewritten as

$$\sum_{j=1}^{d+1} a_j y_j + \sum_{1 \leq j \leq j' \leq d+1} a_{j,j'} y_{j,j'} + a_0 \leq 0.$$

Since the a_j and $a_{j,j'}$ only depend on d_Q , h_0 , and r , and the above equation holds for any y_j and $y_{j,j'}$ implied by an $h \in B_Q(h_0, r)$, then it converts $B_Q(h_0, r)$ into a halfspace in $\mathbb{R}^{d'}$ where $d' = 2(d+1) + \binom{d+1}{2} = \frac{1}{2}(d^2 + 5d + 4)$. Since the VC-dimension of halfspaces in $\mathbb{R}^{d'}$ is $d' + 1$, the VC dimension of $(\mathcal{H}, \mathcal{R}_Q)$ is at most $d' + 1 = \frac{1}{2}(d^2 + 5d + 6)$. \square

Remark. This distance, metric property, and VC-dimension result extend to operate between any objects, such as polynomial models of regression, when linearized to hyperplanes in \mathbb{R}^d .

2.4 Applications in Analysis

The new distance d_Q for hyperplanes has many applications in statistical and algorithmic data analysis where hyperplanes map to linear models. For instance, given a large varieties of regression models $H = \{h_1, h_2, \dots, h_m\}$ (e.g., stemming from different algorithms or model parameters) we can define a Gaussian-like kernel $K(h_1, h_2) = \exp(-d_Q(h_1, h_2)^2)$ and kernel density estimate $\text{KDE}_H(h) = \frac{1}{|H|} \sum_{h_i \in H} K(h, h_i)$. The VC-dimension ν of the metric balls of d_Q implies numerous stability and approximation properties of the KDE. For instance, given a sample $S \subset H$ of size $O(\nu/\epsilon^2)$ ensures that with constant probability $\|\text{KDE}_S - \text{KDE}_H\|_\infty \leq \epsilon$ [13]. The embedding implies we can use Lloyd's algorithm for k -means clustering, and the metric property implies Gonzalez algorithm [11] for k -center clustering will give a 2-approximation.

2.5 Direct Extension (literally) to Trajectories

In this section, we show how d_Q can be simply generalized to the distance between two piecewise-linear curves, while retaining the many nice properties described above. Let $\Gamma_k = \{\gamma \mid \gamma \text{ is a curve in } \mathbb{R}^2 \text{ defined by } k \text{ ordered line segments}\}$ represent the space of all k -piecewise linear curves.

For any curve $\gamma \in \Gamma_k$, let its k segments be $\langle s_1, s_2, \dots, s_k \rangle$, and let these map to k lines ℓ_1, \dots, ℓ_k where each ℓ_j contains s_j (literally an "extension" of s_j to a line ℓ_j , \supset). Next add two more lines: ℓ_0 which is perpendicular to ℓ_1 and passes through the first end point of s_1 , and ℓ_{k+1} which is perpendicular to ℓ_k and passes through the last end point of s_k (in high dimensions, some canonical choice of ℓ_0 and ℓ_{k+1} is needed). We now represent γ as the ordered set of $k+2$ lines $(\ell_0, \ell_1, \dots, \ell_k, \ell_{k+1})$. This mapping is 1to1, since segments s_i and s_{i+1} share a common end point, and this defines the intersection between ℓ_i and ℓ_{i+1} . The intersections with the added lines ℓ_0 and ℓ_{k+1} define first and last endpoints of s_1 and s_k , and these endpoints are sufficient to define γ .

Now for two curves $\gamma^{(1)}, \gamma^{(2)} \in \Gamma_k$, we define the distance using their line representations $(\ell_0^{(1)}, \dots, \ell_{k+1}^{(1)})$ and $(\ell_0^{(2)}, \dots, \ell_{k+1}^{(2)})$, respectively, as

$$d_Q^{\leftrightarrow}(\gamma^{(1)}, \gamma^{(2)}) := \frac{1}{k+2} \left(\sum_{i=0}^{k+1} d_Q(\ell_i^{(1)}, \ell_i^{(2)}) \right).$$

Metric. If $d_Q^{\leftrightarrow}(\gamma^{(1)}, \gamma^{(2)}) = 0$, then $d_Q(\ell_i^{(1)}, \ell_i^{(2)}) = 0$ for all $i \in [k]$, which implies $\ell_i^{(1)} = \ell_i^{(2)}$ if Q is full rank. Combined with the 1to1 nature of the mapping from $\gamma = (s_1, \dots, s_k)$ to $(\ell_0, \dots, \ell_{k+1})$, we have that if Q is full rank, then d_Q^{\leftrightarrow} is a metric over Γ_k .

VC dimension. The distance $d_Q^{\leftrightarrow}(\cdot, \cdot)$ can induce a range space $(\Gamma_k, \mathcal{S}_{Q,k})$, where again Γ_k is the collection of all k -piecewise linear curves in \mathbb{R}^2 , and $\mathcal{S}_{Q,k} = \{B_Q(\gamma, r) \mid \gamma \in \Gamma_k, r \geq 0\}$ with metric ball $B_Q(\gamma, r) = \{\gamma' \in \Gamma_k \mid d_Q^{\leftrightarrow}(\gamma, \gamma') \leq r\}$. Using the straightforward extensions of the method in the proof of Theorem 2.3, we can show the VC dimension of this range space only depends on k , and is

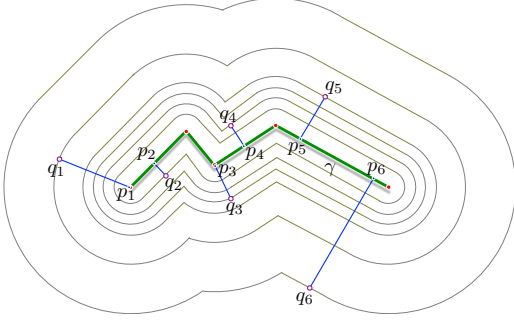


Figure 2: Illustrating q_i and p_i on a trajectory for d_Q and d_Q^π .

independent of the number of points in Q . Specifically, for full rank $Q \subset \mathbb{R}^2$, the VC-dimension of $(\Gamma_k, \mathcal{S}_{Q,k})$ is at most $9k + 19$.

While retaining all above mathematical properties, this distance is unintuitive, and as we show in Section 4, can perform less than optimally. We next develop other trajectory distances which are more intuitive, but have weaker mathematical properties.

3 Landmark Distances Between Trajectories

In this section, we define two variants of d_Q for trajectories, focused on their modeling as piecewise-linear curves on \mathbb{R}^2 . We let Γ define the set of such curves, and they are specified by a series of critical points $\langle c_0, c_1, \dots, c_k \rangle$. The curve $\gamma \in \Gamma$ is the subset of \mathbb{R}^2 defined by the k segments s_1, s_2, \dots, s_k where $s_i = c_{i-1}c_i$ is the continuous set of points between critical points c_{i-1} and c_i . For notational convenience, we will describe all curves as having k segments, but the distance will not require this. Moreover, since we model the trajectory as a continuous subset of \mathbb{R}^2 , it will not distinguish trajectories of different speeds or moving in opposite directions but following the same paths.

Now for a curve $\gamma \in \Gamma$ and size n point set $Q \subset \mathbb{R}^2$, define $v_i = \min_{p \in \gamma} \|q_i - p\|$ and $p_i = \arg \min_{p \in \gamma} \|q_i - p\|$; see Figure 2. For two curves $\gamma^{(1)}$ and $\gamma^{(2)}$ denote these values as $v_i^{(1)}, p_i^{(1)}$ and $v_i^{(2)}, p_i^{(2)}$ respectively. Our distances are then defined as:

$$d_Q(\gamma^{(1)}, \gamma^{(2)}) = \left(\frac{1}{n} \sum_{i=1}^n (v_i^{(1)} - v_i^{(2)})^2 \right)^{\frac{1}{2}},$$

$$d_Q^\pi(\gamma^{(1)}, \gamma^{(2)}) = \frac{1}{n} \sum_{i=1}^n (\|p_i^{(1)} - p_i^{(2)}\|).$$

The standard variant d_Q is the analog of the version for halfspaces, where as the second variant d_Q^π (the *projected landmark distance*) projects Q onto the closest points of the curves, and then computes the average distances with respect to these projected points.

3.1 Metric Properties

In this section, we show a reasonable condition for the trajectories and Q so that both variants are metrics. As with lines and half-spaces, these distances are always pseudometrics: the symmetry and triangle inequality are direct consequences of the embedding to Euclidean space. The only restriction of the trajectories is to ensure that two distinct curves do not have a distance 0, and in our

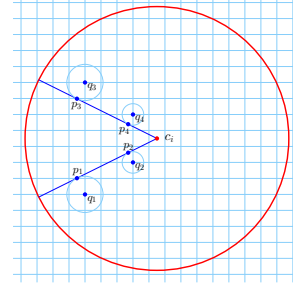


Figure 3: c_i is a critical point of $\gamma^{(1)}$

arguments this requires that the critical points have some non-zero separation from other parts of the curve. These restrictions may not be necessary, but it makes the proofs simple enough. Then we basically just require that Q is sufficiently dense; if we decide many of these points are irrelevant, we can reduce the weights on those points (keeping them non-zero) and the metric properties still hold.

We define a family of curves $\Gamma_\tau \subset \Gamma$ so each $\gamma \in \Gamma_\tau$ has two restrictions: (R1) Each angle $\angle_{[c_{i-1}, c_i, c_{i+1}]}$ about an internal critical point c_i is non-zero (i.e., in $(0, \pi)$). (R2) Each critical point c_i is τ -separated, that is the ball $B(c_i, \tau) = \{x \in \mathbb{R}^2 \mid \|x - c_i\| \leq \tau\}$ only intersects the two adjacent segments s_{i-1} and s_i of γ , or one adjacent segment for end points (i.e., only the s_1 for c_0 and s_k for c_k , if γ has k line segments). The τ -separated property, for instance, enforces that critical points are at least a distance τ apart.

We next restrict that all curves (and Q) lie in a sufficiently large bounded region $\Omega \subset \mathbb{R}^2$. Let $\Gamma_\tau(\Omega)$ be the subset of Γ_τ where all curves γ have all critical points within Ω , and in particular, no $c_i \in \gamma \in \Gamma_\tau(\Omega)$ is within a distance τ of the boundary of Ω . Now for $\eta > 0$, define an infinite grid $G_\eta = \{g_v \in \mathbb{R}^2 \mid g_v = \eta v \text{ for } v = (v_1, v_2) \in \mathbb{Z}^2\}$, where \mathbb{Z} is all integers.

THEOREM 3.1. For $Q = G_\eta \cap \Omega$ and $\eta \leq \frac{\tau}{16}$, both d_Q and d_Q^π are metrics in $\Gamma_\tau(\Omega)$.

PROOF. We prove this theorem for d_Q^π , and the proof for d_Q is similar and given in Appendix B. Suppose $\gamma^{(1)}, \gamma^{(2)} \in \Gamma_\tau(\Omega)$ have critical points c_0, c_1, \dots, c_k and c'_0, c'_1, \dots, c'_k respectively. We only need to show if $d_Q^\pi(\gamma^{(1)}, \gamma^{(2)}) = 0$ then $\gamma^{(1)} = \gamma^{(2)}$. Here, if two piecewise-linear curves have the same critical points and their orders are the same or reverse of each other, then these two curves are regarded as the same curve.

The argument follows 4 steps assuming $d_Q^\pi(\gamma^{(1)}, \gamma^{(2)}) = 0$: (Step 1) Around each critical point c_i of $\gamma^{(1)}$, we can identify at least 4 points q_1, q_2, q_3, q_4 that map to p_1, p_2, p_3, p_4 , two each on the two segments adjacent to c_i . (Step 2) The segments between defined by $\overline{p_1 p_2}$ and $\overline{p_3 p_4}$ must also be part of $\gamma^{(2)}$. (Step 3) The line extension of those two line segment must intersect at c_i , and this must also be critical point on $\gamma^{(2)}$ (Step 4) Because these Steps 1-3 can be repeated for all critical points on $\gamma^{(1)}$ and on $\gamma^{(2)}$, they must share critical points and connecting line segments, and be the same curves.

We formalize these steps based on three observations: (O1) For $q \in Q, \gamma \in \Gamma, p = \arg \min_{p' \in \gamma} \|p' - q\|$, suppose l is the tangent line of the circle $C(q, \|q - p\|)$ where q is center and $\|q - p\|$ its radius, at point p . If $l \cap B(p, \delta)$ is not apart of γ for all $\delta > 0$, then p must be a critical point of γ . (O2) If $\gamma \in \Gamma_\tau$, then in any ball with radius $\frac{\tau}{2}$,

there is at most one critical point of γ . (O3) If a point moves along $\gamma \in \Gamma$, then it can only stop or change direction at critical points.

Step 1: Suppose $c_i = (x_i, y_i)$ ($1 \leq i \leq k-1$) is a critical point of $\gamma^{(1)}$, and consider a ball $B(c_i, \frac{1}{2}\tau)$, as shown in Figure 3. Since the side length of each grid cell is $\eta \leq \frac{1}{16}\tau$, from the τ -separated property (R2) we know for any $q \in Q \cap B(c_i, \frac{\tau}{2})$, $p = \arg \min_{p' \in \gamma^{(1)}} \|p' - q\|$ is in $B(c_i, \frac{\tau}{2})$. So, there exist two points q_1, q_2 that are mapped to points p_1, p_2 on one line segment of $\gamma^{(1)}$ and another two points q_3, q_4 are mapped to points p_3, p_4 on the other line segment of $\gamma^{(1)}$ in $B(c_i, \frac{\tau}{2})$. Since $d_Q^\pi(\gamma^{(1)}, \gamma^{(2)}) = 0$, we know p_1, p_2, p_3, p_4 are also on $\gamma^{(2)}$.

Step 2: We assert the line segment p_1p_2 must be a part of $\gamma^{(2)}$. From (O2), we know p_1 and p_2 cannot both be the critical point of $\gamma^{(2)}$ at the same time, so we assume p_1 is not a critical point. Thus, from (O1) we know a small part of tangent line l of circle $C(q_1, \|q_1 - p_1\|)$ at p_1 is a part of $\gamma^{(2)}$. If p_2 is a critical point of $\gamma^{(2)}$, then from (O3) and (O2) we know the line segment p_1p_2 must be a part of $\gamma^{(2)}$. If p_2 is not a critical point of $\gamma^{(2)}$, then from (O1) we know a small part of tangent line l of circle $C(q_1, \|q_1 - p_1\|)$ at p_2 is a part of $\gamma^{(2)}$. So, in this case, (O3) and (O2) implies the line segment p_1p_2 is a part of $\gamma^{(2)}$. Using a similar argument, we know the line segment p_3p_4 is also a part of $\gamma^{(2)}$.

Step 3: We extend the line $\overline{p_1p_2}$ from p_1 to p_2 and the line $\overline{p_3p_4}$ from p_3 to p_4 . Suppose they intersect with the boundary of $B(c_i, \frac{\tau}{2})$ at p'_2 and p'_4 respectively. Since $\gamma^{(2)}$ cannot go into the interior of any ball with centers in $Q \cap B(c_i, \frac{\tau}{2})$, from (O3) we know there must be one critical point in line segment $p_2p'_2$. For the same reason, there must be one critical point in line segment $p_4p'_4$. Thus, (O2) implies c_i is a critical points of $\gamma^{(2)}$.

Step 4: Considering that $\gamma^{(2)}$ has to pass through p_1, p_2, p_3, p_4 and c_i , from τ -separated property (R2), we know $\gamma^{(1)}$ and $\gamma^{(2)}$ must overlap with each other in $B(c_i, \frac{\tau}{2})$. For two endpoints c_0 and c_k we can make the same argument, which means in a neighborhood of each critical point of $\gamma^{(1)}$, $\gamma^{(1)}$ overlaps with $\gamma^{(2)}$. This means $\{c_0, c_1, \dots, c_k\}$ is a subset of $\{c'_0, c'_1, \dots, c'_k\}$. Using the same argument $\{c'_0, c'_1, \dots, c'_k\}$ is a subset of $\{c_0, c_1, \dots, c_k\}$. Therefore, $k = k'$ and we know $\gamma^{(1)}$ and $\gamma^{(2)}$ must have the same critical points and their orders must be the same or reverse of each other. \square

Remark. We did not try to optimize constants. The point is that for most families of trajectories, with Q sufficiently dense our distances are metrics, not just pseudometrics. In practice these distances will work for small sets Q (see below).

4 Trajectories Analysis via New Distances

We demonstrate that d_Q and d_Q^π (and to lesser extent d_Q^{\leftrightarrow}) work effectively on real world problems. These approaches achieve state-of-the-art performance, are incredibly simple to use, and their sketched representation plugs directly into k -means clustering, KNN or SVM classifiers, or ANN libraries. We show that only a small number of landmarks are needed for good accuracy, and when certain landmarks are especially meaningful, our approaches can be easily tuned to achieve very high accuracy.

4.1 Related Trajectory Distances, and Landmarks

There are by now numerous definitions of trajectories, with a variety of different aspects they can model and take into account.

We compare the classification errors found using d_Q^{\leftrightarrow} , d_Q and d_Q^π with a series of representative distances for trajectories. These are: Euclidean distance among the critical points (Eu) [25], discrete Frechet distance (dF) [6], dynamic time warping distance (DTW) [24], discrete Hausdorff distance (dH) [16], longest common subsequence distance (LCSS) [21], edit distance for real sequences (EDR) [4]. We also compare against the recently proposed locality sensitive hashing distance (LSH1 $_Q$), and the ordered version of locality sensitive hashing distance (LSH2 $_Q$) [3], which consider the intersection of the trajectories with a set of disks. This is conceptually similar to our methods, where we can think of the landmarks Q as the centers of disks (as we do in experiments), and their approach requires a radius parameter r for all disks, and is not a metric. The definitions of these distances are given in Appendix C.

To find the best parameters to minimized the error, for LCSS we tested $\epsilon \in \{0.001, 0.005, 0.01, 0.015, \dots, 0.055\}$, $\delta \in \{1, 2, 3, \dots, 10\}$, and for EDR we tested $\epsilon \in \{0.001, 0.005, 0.01, 0.015, \dots, 0.055\}$, and for LSH1 $_Q$ and LSH2 $_Q$ we tested $r \in \{0.005, 0.01, 0.02, \dots, 0.11\}$. Since in all experiments (except Section 4.6), each trajectory is represented by a sequence of 10 critical points, it is enough to take the largest value of δ as 10 for LCSS. We only show the best results in this section, but provide the results of other parameter settings in Appendix D.2.

Zhang *et al.* [25] conducted a large comparison of trajectory distances and showed that in most cases Eu is general enough, efficient, and a superior or nearly as good model as any other ; we include dF and DTW as examples which search over all possible alignments and thus do not require the same number of or aligned critical points on both curves. The restriction that trajectories have the same number of critical points is also not required for dH, EDR, LSH1 $_Q$, and LSH2 $_Q$, but in comparisons we always first reduce all trajectories to 10 critical points (with Douglas-Peucker), except in Section 4.6, so a fair comparison to all metrics can be made.

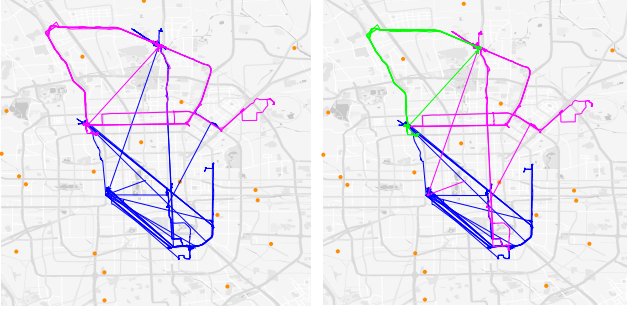
Even beyond the recent trajectory LSH paper [3], the use of waypoints to provide a distance between trajectories is not new. However, they are typically used in other contexts, such as annotating with geolocated social media [22]. Or for instance, in the context of a line of work [8, 12, 15] seeking to find the k nearest time-encoded trajectories to a given point at a specific time, Lin *et al.* [15] use a set of landmarks Q to map trajectories and query points into the Voronoi cells of Q to quickly help in pruning.

4.2 Warm-up: k -means Clustering

As a warm up, we consider clustering the 42 trajectories from user id_{155} in the Geolife GPS trajectory dataset [26]. We randomly choose 20 spread-out Beijing POIs as the landmark set Q , shown as orange dots in Figure 4. Using d_Q , this maps each trajectory γ to \mathbb{R}^{20} , and we directly run Lloyd's algorithm for k -means clustering with $k = 2, 3$, and color-code the corresponding trajectories in Figure 4. We observe that although the trajectories are intertwined, there is a central-city cluster found in both cases, and either 1 or 2 clusters found on the north side.

Table 1: Classification error on Beijing Drivers with KNN.

best param	d_Q^{\leftrightarrow}	d_Q	d_Q^π	Eu	dF	DTW	dH	LCSS	EDR	LSH1 $_Q$	LSH2 $_Q$
	-	-	-	-	-	-	-	$\epsilon=0.005, \delta=10$	$\epsilon=0.005$	$r=0.06$	$r=0.1$
mean	0.1703	0.0817	0.0724	0.0811	0.1045	0.0722	0.0883	0.0714	0.0802	0.1290	0.2409
median	0.1458	0.0667	0.0581	0.0654	0.0873	0.0571	0.0722	0.0500	0.0554	0.0949	0.2182
variance	0.0108	0.0039	0.0033	0.0040	0.0054	0.0036	0.0043	0.0054	0.0070	0.0128	0.0210

**Figure 4: 2 or 3 clusters (color-coded) under k -means on d_Q with 20 landmarks Q shown overlaid on Beijing.**

4.3 Classifying Trajectories 1: Beijing Drivers

We also consider classifying trajectories from users in the Geolife dataset [26] with the same 20 POI landmarks Q as in the clustering example. There are 182 users, and each user has several trajectories in Beijing. We only consider those trajectories with more than 10 critical points, and if a user has less than 10 such trajectories, then we remove this user. Thus, 54 users are removed, and in the remaining 128 users, 20 of them have more than 200 trajectories. For each of these users, we just randomly sample 200 trajectories (without replacement), to avoid severe imbalance in classification – dealing with the imbalance challenge is not the focus of this paper.

Suppose two users with id_1 and id_2 have two sets of trajectories $\Gamma^{(1)}$ and $\Gamma^{(2)}$ respectively. Letting $|\Gamma^{(1)}| = m_1$ and $|\Gamma^{(2)}| = m_2$, we randomly sample $\lfloor \frac{3m_1}{10} \rfloor$ trajectories from $\Gamma^{(1)}$ and $\lfloor \frac{3m_2}{10} \rfloor$ trajectories from $\Gamma^{(2)}$ respectively to form a test set, and use the other trajectories in $\Gamma^{(1)} \cup \Gamma^{(2)}$ as the training data. Then we choose an algorithm and metric to do classification, and compute the error. For users with id_1 and id_2 , we do this 10 times and take the mean error as $error(id_1, id_2)$. We compute $error(id_1, id_2)$ for all 8128 pairs

of 128 uses, and then output the mean, median, and variance of these 8128 errors.

For all of these 10 distances, we use the KNN classification ($K = 5$); see Table 1. The lowest error rates of about 7% error is achieved by d_Q^π , DTW and LCSS; they are within the variance bounds of each other. Then d_Q , Eu, and EDR achieve error about 8%, again within the error bounds of each other. Other metrics perform worse with for example, dF at 10%, LSH1 $_Q$ at 13%, d_Q^{\leftrightarrow} at 17%, and LSH2 $_Q$ at 24% error.

For d_Q , d_Q^π and Eu, since they map a trajectory to a vector in Euclidean space, we can also directly use SVM to classify these vectors. We use `fitsvm` in matlab R2018b and set ‘IterationLimit’ (the maximum iteration number) as 200,000 for all kernel functions, and set ‘KernelScale’ as ‘auto’ for Gaussian kernel. From Table 2, we can see for SVM with three kinds of kernel functions, both d_Q and d_Q^π are better than Eu. In the case of Gaussian SVM, both d_Q and d_Q^π achieve an error rate of about 7% which is less than the about 8% achieved by Eu, and this difference is larger than the variances. Again in this SVM setting d_Q^{\leftrightarrow} performs much worse (for Gaussian kernels) or comparable to other measures, about the same as Eu, (linear quadratic kernels).

As we increase the size of Q to 200 (chosen at random), then both d_Q and d_Q^π slightly improve in performance, but not drastically, and d_Q^{\leftrightarrow} performs about the same. The error statistics is shown in Table 3, from which we can see for KNN, the performance of d_Q is better than Euclidean distance, and d_Q^π provides the smallest error (mean error 0.0708, smaller than 0.0714 of LCSS). Moreover, we can see as $|Q|$ increases, the error of d_Q and d_Q^π with three kernel functions all decrease, except d_Q^π with quadratic kernel. When we use quadratic kernel, the algorithm takes a long time to converge, and for $|Q| = 200$, the dimension of vectors used in d_Q^π is 400, so the algorithm may not converge within 200000 iterations. The relatively small improvement also demonstrates that even with a small size, random Q , the distances still perform at or near the state-of-the-art.

Table 2: Classification error on Beijing Drivers with SVM.

kernel	statistics	d_Q^{\leftrightarrow}	d_Q	d_Q^π	Eu
linear	mean	0.2170	0.2066	0.2046	0.2173
	median	0.1987	0.1851	0.1892	0.2000
	variance	0.0140	0.0158	0.0149	0.0164
quadratic	mean	0.2327	0.2190	0.2000	0.2377
	median	0.2000	0.1778	0.1455	0.1949
	variance	0.0200	0.0281	0.0284	0.0278
Gaussian	mean	0.1725	0.0727	0.0733	0.0845
	median	0.1509	0.0587	0.0588	0.0690
	variance	0.0110	0.0035	0.0036	0.0045

Table 3: Classification error on Beijing with $|Q| = 200$.

	statistics	KNN	linear-SVM	quad-SVM	Gauss-SVM
d_Q	mean	0.0801	0.1419	0.1398	0.0722
	median	0.0650	0.1125	0.0909	0.0581
	variance	0.0038	0.0112	0.0203	0.0035
d_Q^π	mean	0.0708	0.1432	0.2606	0.0726
	median	0.0558	0.1179	0.2222	0.0583
	variance	0.0033	0.0104	0.0373	0.0036
d_Q^{\leftrightarrow}	mean	0.1711	0.2362	0.2673	0.1735
	median	0.1471	0.2200	0.2460	0.1529
	variance	0.0108	0.0138	0.0212	0.0110

4.4 Classifying Trajectories 2: Bus versus Car

As another example, we consider the GPS Trajectories Data Set [5] in UCI machine learning repository. There are 87 car trajectories, and 76 bus trajectories in Aracaju, a city of Brazil. We remove those trajectories having less than 10 critical points, and then 78 car trajectories and 45 bus trajectories are left. For these 123 trajectories are shown in Figure 5(Left), where pink curves are car trajectories and blue curves are bus trajectories. We hand-pick 10 points as Q_1 such that each point is close to one class of trajectories, and randomly generate 20 points as Q_2 . Each time we randomly choose 23 car trajectories and 13 bus trajectories as test data, and use other trajectories as training data to perform classification experiments,

Table 4: Classification error on Bus vs. Car.

	distance	mean	median	variance
KNN	$d_{Q_1}^{\leftrightarrow}$	0.2027	0.1944	0.0042
	$d_{Q_2}^{\leftrightarrow}$	0.2148	0.2222	0.0039
	d_{Q_1}	0.2331	0.2222	0.0045
	d_{Q_2}	0.2229	0.2222	0.0041
	$d_{Q_1}^{\pi}$	0.2608	0.2500	0.0039
	$d_{Q_2}^{\pi}$	0.2505	0.2500	0.0039
	Eu	0.3323	0.3333	0.0044
	dF	0.3431	0.3333	0.0045
	DTW	0.3118	0.3056	0.0046
	dH	0.3284	0.3333	0.0039
	LCSS ($\epsilon=0.015, \delta=3$)	0.2448	0.2500	0.0037
	EDR ($\epsilon=0.015$)	0.2640	0.2500	0.0039
	LSH1 $_{Q_1}$ ($r=0.02$)	0.2673	0.2778	0.0020
	LSH2 $_{Q_1}$ ($r=0.08$)	0.2516	0.2500	0.0022
	LSH1 $_{Q_2}$ ($r=0.03$)	0.2209	0.2222	0.0039
	LSH2 $_{Q_2}$ ($r=0.05$)	0.2690	0.2778	0.0022
	linear SVM	Eu	0.3624	0.3611
$d_{Q_1}^{\leftrightarrow}$		0.3652	0.3611	0.0002
$d_{Q_2}^{\leftrightarrow}$		0.3655	0.3611	0.0002
d_{Q_1}		0.3611	0.3611	0
d_{Q_2}		0.3611	0.3611	0
$d_{Q_1}^{\pi}$		0.3611	0.3611	0
$d_{Q_2}^{\pi}$		0.3612	0.3611	0.000003
quadratic SVM	Eu	0.3609	0.3611	0.0044
	$d_{Q_1}^{\leftrightarrow}$	0.3645	0.3611	0.0004
	$d_{Q_2}^{\leftrightarrow}$	0.3140	0.3056	0.0017
	d_{Q_1}	0.3617	0.3611	0.00003
	d_{Q_2}	0.3625	0.3611	0.00008
	$d_{Q_1}^{\pi}$	0.2644	0.2500	0.0042
	$d_{Q_2}^{\pi}$	0.2828	0.2778	0.0045
Gaussian SVM	Eu	0.2239	0.2222	0.0034
	$d_{Q_1}^{\leftrightarrow}$	0.1940	0.1944	0.0031
	$d_{Q_2}^{\leftrightarrow}$	0.2120	0.2222	0.0032
	d_{Q_1}	0.1894	0.1944	0.0029
	d_{Q_2}	0.1968	0.1944	0.0033
	$d_{Q_1}^{\pi}$	0.1659	0.1667	0.0033
	$d_{Q_2}^{\pi}$	0.1731	0.1667	0.0033

and compute the error. We do this 1000 times and then compute the mean, median and variance of the error for each algorithm.

The results are shown in Table 4, and we see the KNN classification results using all 14 distance, using either Q_1 (10 chosen near data) or Q_2 (20 randomly chosen). The results are slightly better for Q_2 in almost all distances d_Q , d_Q^{π} , LSH1 $_Q$, and LSH2 $_Q$ – except d_Q^{\leftrightarrow} . In these experiments on Q_2 , the best mean error (about 21% to 22%) is achieved by d_Q^{\leftrightarrow} , d_Q , and LSH1 $_Q$ (which required a parameter search). The best error is about 20% by d_Q^{\leftrightarrow} using Q_2 . While d_Q^{π} , LCSS, EDR, and LSH2 $_Q$ achieve error between 25% and 27%. Noticeably, the methods which were competitive with d_Q and d_Q^{π} on the Beijing Drivers data are EDR, which required a parameter tuned, as well as DTW and Eu, which now have error rate above 31%. As a baseline, always predicting “car” obtains 36% error.

We show the results of applying SVM in Table 4. Again the difference is small between Q_2 and Q_1 . And while the linear and quadratic SVM do not perform that well; for the Gaussian kernel on d_Q and d_Q^{π} the mean error is only 16% to 20%, and 19% to 21% for d_Q^{\leftrightarrow} . The overall best is $d_{Q_1}^{\pi}$ achieving a mean error of 16.59%.

4.5 Classifying Trajectories 3: Landmark-Sensitivity

To show the further advantage of d_Q and d_Q^{π} , we create a synthetic data set that appears random, except one set of trajectories pass nearby a POI and the others do not. We randomly generate two classes of trajectories on the map of Beijing, and each class has 30 trajectories. Each trajectory has 10 critical points, and all blue trajectories passes through some point close to the city center, and all pink trajectories do not. We hand-pick a point at the Palace Museum, the center of the city, and randomly choose other 9 points to form the set Q . As shown in Figure 5(Right), these trajectories are a mess and largely indistinguishable, except that the blue set passes near the landmark: Palace Museum. We next show that d_Q and d_Q^{π} which are landmark-aware (e.g., POI-aware) have significantly more power in distinguishing these classes.

We randomly choose 21 trajectories from each class to form a training data set of size 42, and use the other trajectories as test data. Each time, we record the error, and repeat this 1000 times to output the mean, median and variance of these errors.

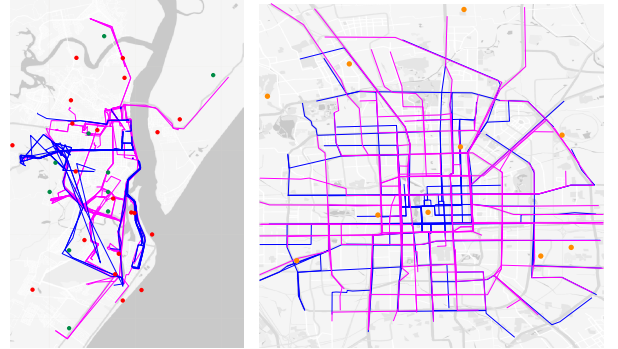


Figure 5: Left: Bus (blue) and car (pink) trajectories with landmark sets Q_1 (green points), Q_2 (red points). Right: Two classes of trajectories and Q (orange points).

Table 5 shows the KNN classification results. Distances Eu and dF provide no advantage over a random classifier (which would report error 0.5). d_Q^π , d_Q , d_Q^{\leftrightarrow} , DTW, and Hausdorff achieve only slight advantage over random classifiers, with error rates about 43% to 48%, with the best achieved by d_Q^π . This extends to the SVM approaches in Table 6. The best parameter free approach is d_Q^π at 43.85% error. The parameterized distances LCSS, EDR, LSH1 $_Q$, and LSH2 $_Q$ perform better with error rates 25% to 40%; but these can be sensitive to the parameter choices – we only show the best results.

Next we can consider re-weighting the importance of the landmarks Q , for instance in the case where one particular POI (in this case q_1) is known to have a specific meaning in the classification task (e.g., did someone stop by the sporting event, or a military point of interest). Suppose $w_i > 0$ is a weight of $q_i \in Q$, and $W = (w_1, w_2, \dots, w_n)$. Then we can generalize the definitions to:

$$d_{Q,W}(Y^{(1)}, Y^{(2)}) = \left(\sum_{i=1}^n w_i (d_i^{(1)} - d_i^{(2)})^2 \right)^{\frac{1}{2}},$$

$$d_{Q,W}^\pi(Y^{(1)}, Y^{(2)}) = \sum_{i=1}^n w_i (\|p_i^{(1)} - p_i^{(2)}\|).$$

Table 5: Landmark-sensitive classification error with KNN.

	distance	mean	median	variance
	Eu	0.5226	0.5000	0.0100
	dF	0.5056	0.5000	0.0096
	DTW	0.4777	0.5000	0.0107
	dH	0.4627	0.4444	0.0105
LCSS ($\epsilon = 0.001, \delta = 8$)		0.3437	0.3333	0.0066
	EDR($\epsilon = 0.02$)	0.3916	0.3889	0.0068
	LSH1 $_Q$ ($r=0.01$)	0.2524	0.2222	0.0098
	LSH2 $_Q$ ($r=0.02$)	0.3248	0.3333	0.0084
	d_Q	0.4729	0.5000	0.0101
	$d_{Q,W}$ ($w_1 = 0.3$)	0.4133	0.3889	0.0111
	$d_{Q,W}$ ($w_1 = 0.6$)	0.2687	0.2778	0.0094
	$d_{Q,W}$ ($w_1 = 0.9$)	0.0592	0.0556	0.0037
	d_Q^π	0.4385	0.4444	0.0092
	$d_{Q,W}^\pi$ ($w_1 = 0.3$)	0.3846	0.3889	0.0085
	$d_{Q,W}^\pi$ ($w_1 = 0.6$)	0.2396	0.2222	0.0065
	$d_{Q,W}^\pi$ ($w_1 = 0.9$)	0.1002	0.0556	0.0067
	d_Q^{\leftrightarrow}	0.4711	0.4444	0.0106
	$d_{Q,W}^{\leftrightarrow}$ ($w_1 = 0.3$)	0.4468	0.4444	0.0113
	$d_{Q,W}^{\leftrightarrow}$ ($w_1 = 0.6$)	0.4377	0.4444	0.0112
	$d_{Q,W}^{\leftrightarrow}$ ($w_1 = 0.9$)	0.4466	0.4444	0.0100

Table 6: Landmark-sensitive classification error with SVM.

kernel	statistics	d_Q^{\leftrightarrow}	d_Q	d_Q^π	Eu
linear	mean	0.5000	0.4586	0.4941	0.5887
	median	0.5000	0.4444	0.5000	0.6111
	variance	0.0095	0.0097	0.0099	0.0085
quadratic	mean	0.5403	0.4617	0.5574	0.4795
	median	0.5556	0.4444	0.5556	0.5000
	variance	0.0092	0.0094	0.0101	0.0112
Gaussian	mean	0.5059	0.4567	0.4556	0.5906
	median	0.5000	0.4444	0.4444	0.6111
	variance	0.0092	0.0089	0.0099	0.0088

Let $w_1 \in (0, 1)$ be the weight of q_1 , and $w_i = \frac{1}{9}(1 - w_1)$ (for $2 \leq i \leq 10$) be the weight of all other points in Q .

Now observe in Table 5 that the landmark-based distance using a KNN classifier can achieve very low error (6% for $d_{Q,W}$ and 10% for $d_{Q,W}^\pi$) as we gradually increase the weight of the point q_1 from $w_1 = 0.1$ (i.e., d_Q or d_Q^π) to $w_1 = 0.9$ to emphasize a desired POI. The result is even more pronounced for the Gaussian SVM, as shown in Table 7; similar plots are shown for linear and quadratic kernels in Appendix D.1. As w_1 is increased from (uniform) 0.1 to 0.9, the mean error decreases from 45% to 1.5% for $d_{Q,W}$ and from 45% to 3% for $d_{Q,W}^\pi$. Thus, while all other distances we tried are only slightly better than random unless their parameters are tuned, by emphasizing a particular POI (a very intuitive adjustment), we achieve almost no error in classifying these trajectories.

4.6 Using d_Q in Nearest Neighbor Search

We demonstrate that d_Q 's sketched representation of the trajectories in $\mathbb{R}^{|Q|}$ allows for *extremely efficient k-nearest neighbor search*. We consider two representative methods [19, 23] for comparison; but do all, e.g., [7]) which require timing information.

As a first comparison, consider a recent heavily-optimized kNN search algorithm focusing on Hausdorff and dF distances [23]; this system, DFT, is optimized for distributed algorithms on a cluster, but show results on 1 node which we compare against. We obtained a random sample of the GEN-TRAJ data set containing $m = 3$ million trajectories, using 36GB of storage (larger than their 30.9GB dataset [23]). From *their* Figure 10, their indexes take 2000 to 6000 sec to build, and kNN queries require 50 to 200 seconds for $k = 10$.

Another distributed system DITA [19] for trajectory similarity search focuses on DTW, returning all trajectories within a threshold. In their [19] Figures 7(a) and 8(a), using 256 cores they achieve query time between 0.001 and 0.01 seconds on Beijing (10.4GB) and Chengdu (28GB) datasets.

To perform kNN queries using d_Q we can sketch trajectories as $|Q|$ -dimensional vectors and use Euclidean distance. Hence, once we create the sketches, we can use any of the highly optimized packages for kNN Euclidean queries (c.f., <http://ann-benchmarks.com>); we choose a consistent top performer K-Graph (<https://github.com/aalgo/kgraph>) with settings: recall=0.99 and max_iteration=50. We run on a desktop with a 6-core Intel Xeon CPU ES-1650 v3 @3.5GHz processor, and 128GB RAM; the same processor as in DFT [23].

Table 7: Landmark-sensitive classification error with weighted Gaussian SVM.

metrics	mean	median	variance
$d_{Q,W}$ ($w_1 = 0.3$)	0.1487	0.1667	0.0065
$d_{Q,W}$ ($w_1 = 0.6$)	0.0303	0	0.0014
$d_{Q,W}$ ($w_1 = 0.9$)	0.0159	0	0.0007
$d_{Q,W}^\pi$ ($w_1 = 0.3$)	0.2997	0.2778	0.0088
$d_{Q,W}^\pi$ ($w_1 = 0.6$)	0.1053	0.1111	0.0049
$d_{Q,W}^\pi$ ($w_1 = 0.9$)	0.0316	0	0.0015
$d_{Q,W}^{\leftrightarrow}$ ($w_1 = 0.3$)	0.4942	0.5000	0.0095
$d_{Q,W}^{\leftrightarrow}$ ($w_1 = 0.6$)	0.4726	0.5000	0.0095
$d_{Q,W}^{\leftrightarrow}$ ($w_1 = 0.9$)	0.4687	0.4444	0.0095

Table 8: The running time experiment of KNN search.

	$ Q $	12	20	28	36	44	52
preprocessing time (s)		38	62	88	114	138	160
sketch size (MB)		337	560	785	1012	1331	1536
index time (s)		106	109	114	119	124	129
index file size (MB)		999	999	1005	1002	1007	1001
query time (10^{-4} s)		4.2	3.7	4.2	3.2	3.5	3.7

For experiments, we randomly choose a set of landmarks among the trajectories with $|Q| = \{12, 20, 28, 36, 44, 52\}$. From these Q we preprocess the data to derive $m \times |Q|$ sketches, a txt file we pass to K-Graph. Then K-Graph builds an index, and allows queries. The preprocessing time (to build sketch), sketch file size, time to build K-Graph’s index, that index size, and the average query time are shown in Table 8. For all these different values of $|Q|$, the K-Graph algorithm reaches recall=0.99 within 7 iterations.

The preprocessing and index building times take 38 to 160 seconds and 106 to 129 seconds, respectively. By comparison, it takes 673 seconds to load the raw data into memory. Combined they are an order of magnitude faster than the index build time for Hausdorff in DFT [23]. The sketch size is only 300 to 1500 MB, and the index sizes are 1000 MB; reducing the size by 1 or 2 orders of magnitude from the original size. Finally, the query times are only 0.00032 to 0.00042 seconds; that is 5 orders of magnitude faster than the DFT index optimized for Hausdorff distance! and 1 to 2 orders of magnitude faster than DITA optimized for DTW and using 256 cores on smaller data. Thus, using d_Q (and existing libraries) allows for small data sketches, and extremely efficient kNN queries.

5 Conclusion and Discussion

We introduce a new family of landmark-based distances d_Q , with applications to trajectories and hyperplanes (regressors, separators). These have nice mathematical properties, e.g., being pseudo-metrics, metrics, and bounded VC-dimension metric balls. On trajectories, new metrics d_Q and d_Q^π are the most general and best or competitive against all other distances in *all* analysis tasks; see Table 9.

The landmark set Q can be randomly chosen and small, or its points can hold specific meaning in which case, the interpretation and discriminatory ability of the distances are greatly enhanced. A companion paper [18] provides an in depth theoretical study of how many landmarks are required to preserve certain errors, how to chose them, and when curves can be explicitly recovered from them. In the present paper, we simply empirically show that in most cases 20 random landmarks are sufficient.

Table 9: Distances on analysis tasks as: best •, competitive •, near competitive ◦; possible ✓ or possible but slower ✓.

task	d_Q	d_Q^π	d_Q^{\leftarrow}	Eu	dF	DTW	dH	LCSS	EDR	LSH $_Q$
easy clust	✓	✓	✓	✓	-	-	-	-	-	-
learn 1	•	•	-	•	◦	•	•	•	•	-
learn 2	•	•	◦	◦	-	•	-	◦	•	◦
learn 3	•	•	-	-	-	-	-	-	-	-
fast NN	✓	✓	✓	✓	-	✓	-	-	-	✓
any k	✓	✓	-	-	✓	✓	✓	✓	✓	✓

These provide meaningful *vectorized representations*. They are general and simple to compute and work with. We believe many applications of these sorts of vectorized distances will be discovered. And there are more mathematical questions to ask about the geometric and statistical power of these landmark-based distances.

Software. Code for reproducing experiments in Section 4 is available here https://drive.google.com/open?id=1Z_NaInfoM_We8b1FnTU5UVuOYcjbP-j

References

- [1] Helmut Alt and Leonidas J. Guibas. 1996. Discrete Geometric Shapes: Matching, Interpolation, and Approximation: A Survey. In *Handbook of Computational Geometry*. -.
- [2] Helmut Alt, Kurt Mehlhorn, Hubert Wagener, and Emo Welzl. 1988. Congruence, Similarity, and Symmetries of Geometric Objects. *DCG* 3 (1988), 237–256.
- [3] Maria Astefanoaei, Paul Cesaretti, Panagiota Katsikouli, and Mayank Goswami andRik Sarkar. 2018. Multi-resolution sketches and locality sensitive hashing for fast trajectory processing. In *SIGSPATIAL*.
- [4] Lei Chen, , M. Tamer Özsu, and Vincent Oria. 2005. Robust and fast similarity search for moving object trajectories. In *SIGMOD*.
- [5] Michael O. Cruz, Hendrik Macedo, R. Barreto, and Adolfo Guimaraes. 2016. *GPS Trajectories Data Set*. <https://archive.ics.uci.edu/ml/datasets/GPS+Trajectories>
- [6] Thomas Eiter and Heikki Mannila. 1994. *Computing Discrete Frechet Distance*. Technical Report. Christian Doppler Laboratory for Expert Systems.
- [7] Yixiang Fang, Reynold Cheng, Wenbin Tang, Silviu Maniu, and Xuan S. Yang. 2016. Scalable algorithms for nearest-neighbor joins on big trajectory data. In *ICDE*.
- [8] Elias Frenzos, Kostas Gratsias, Nikos Pelekis, and Yannis Theodoridis. 2005. Nearest Neighbor Search on Moving Object Trajectories. In *SSTD*.
- [9] Elmer G. Gilbert and Chek-PenG Foo. 1990. Computing the distance between general convex objects in three-dimensional space. *IEEE Trans. Robot. & Autom.* 6 (1990), 53–61.
- [10] E. G. Gilbert, D. W. Johnson, and S. S. Keerthi. 1988. A fast procedure for computing the distance between objects in three-dimensional space. *IEEE Trans. Robot. & Autom.* 4 (1988), 193–203.
- [11] Teofilo F. Gonzalez. 1985. Clustering to Minimize the Maximum Intercluster Distance. *TCS* 38 (1985), 293–306.
- [12] Ralf Hartmut Güting, Thomas Behr, and Jianqiu Xu. 2010. Efficient k-nearest neighbor search on moving object trajectories. In *VLDB*.
- [13] Sarang Joshi, Raj Varma Kommaraju, Jeff M. Phillips, and Suresh Venkatasubramanian. 2011. Comparing Distributions and Shapes Using the Kernel Distance. *SOCG* (2011).
- [14] Yi Li, Philip M. Long, and Aravind Srinivasan. 2001. Improved Bounds on the Samples Complexity of Learning. *JCSS* 62 (2001), 516–527.
- [15] Dan Lin, Rui Zhang, and Aoying Zhou. 2006. Indexing Fast Moving Objects for kNN Queries Based on Nearest Landmarks. *GeoInformatica* 10 (2006), 423–445.
- [16] Facundo Mémoli. 2008. Gromov–Hausdorff distances in Euclidean spaces. *Non-rigid shape analysis and deformable image registration Workshop* (2008).
- [17] Jeff M. Phillips and Pingfan Tang. 2019. *Simple Distances for Trajectories via Landmarks*. Technical Report. arXiv:1804.11284.
- [18] Jeff M. Phillips and Pingfan Tang. 2019. *Sketched MinDist*. Technical Report. (forthcoming).
- [19] Zeyuan Shang, Guoliang Li, and Zhifeng Bao. 2018. DITA: Distributed in-memory trajectory analytics. In *SIGMOD*.
- [20] Vladimir Vapnik and Alexey Chervonenkis. 1971. On the Uniform Convergence of Relative Frequencies of Events to their Probabilities. *Th. Probab. & App.* 16 (1971), 264–280.
- [21] Michail Vlachos, George Kollios, and Dimitrios Gunopulos. 2002. Discovering similar multidimensional trajectories. In *ICDE*.
- [22] Fei Wu, Zhenhui Li, Wang-Chien Lee, Hongjian Wang, and Zhuojie Huang. 2015. Semantic Annotation of Mobility Data using Social Media. In *WWW*.
- [23] Dong Xie, Feifei Li, and Jeff M. Phillips. 2017. Distributed trajectory similarity search. In *VLDB*.
- [24] Byoung-Kee Yi, H.V. Jagadish, and Christos Faloutsos. 1998. Efficient retrieval of similar time sequences under time warping. In *ICDE*.
- [25] Zhang Zhang, Kaiqi Huang, and Tieniu Tan. 2006. Comparison of similarity measures for trajectory clustering in outdoor surveillance scenes. In *ICPR*.
- [26] Yu Zheng, Hao Fu, Xing Xie, Wei-Ying Ma, and Quannan Li. 2011. *Geolife GPS trajectory dataset - User Guide*. <https://www.microsoft.com/en-us/research/publication/geolife-gps-trajectory-dataset-user-guide/>

Appendix. A full version with appendix for extended proofs and more experimental details available here [17].

A Metric Property for Unsigned Variant on the Distance

Suppose $Q = \{q_1, q_2, \dots, q_n\} \subset \mathbb{R}^2$, $\ell_1, \ell_2 \in \mathcal{L} = \{\ell \mid \ell \text{ is a line in } \mathbb{R}^2\}$. Given $\ell \in \mathcal{L}$, we write ℓ in the form as before and define $\bar{v}_Q(\ell) = (\bar{v}_{Q_1}(\ell), \bar{v}_{Q_2}(\ell), \dots, \bar{v}_{Q_n}(\ell))$ where $\bar{v}_{Q_i}(\ell) = |u_1 x_i + u_2 y_i + u_3|$ and (x_i, y_i) is the coordinates of $q_i \in Q$, and then define the first variant of d_Q as

$$\begin{aligned} \bar{d}_Q(\ell_1, \ell_2) &:= \left\| \frac{1}{\sqrt{n}} (\bar{v}_Q(\ell_1) - \bar{v}_Q(\ell_2)) \right\| \\ &= \left(\sum_{i=1}^n \frac{1}{n} (\bar{v}_{Q_i}(\ell_1) - \bar{v}_{Q_i}(\ell_2))^2 \right)^{\frac{1}{2}}. \end{aligned} \quad (3)$$

For (3), we have the following theorem.

THEOREM A.1. *Suppose in $Q \subset \mathbb{R}^2$ there is a subset of five points, and any three points in this subset are non-collinear, then \bar{d}_Q is a metric in \mathcal{L} .*

PROOF. We only need to show if $\bar{d}_Q(\ell_1, \ell_2) = 0$, then $\ell_1 = \ell_2$. Suppose $\bar{Q} = \{q_1, \dots, q_5\} \subset Q$, and any three points in \bar{Q} are not on the same line. If $\ell_1 \neq \ell_2$, then let ℓ'_1 and ℓ'_2 be the two bisectors of the angles formed by ℓ_1 and ℓ_2 . From $\bar{d}_Q(\ell_1, \ell_2) = 0$, we know $\bar{v}_{Q_i}(\ell_1) = \bar{v}_{Q_i}(\ell_2)$ for $i \in [5]$, which means the distances from $q_i \in \bar{Q}$ to ℓ_1 and to ℓ_2 are equal. So, any point $q_i \in \bar{Q}$ must be either on ℓ'_1 or on ℓ'_2 , which implies there must be three collinear points in \bar{Q} . This is contradictory to the fact that any three points in \bar{Q} are not on the same line. \square

Remark. Definition (3) can be generalized to hyperplanes in \mathbb{R}^d :

$$\bar{d}_Q(h_1, h_2) := \left(\sum_{i=1}^n \frac{1}{n} (\bar{v}_{Q_i}(h_1) - \bar{v}_{Q_i}(h_2))^2 \right)^{\frac{1}{2}}, \quad (4)$$

where $h_1, h_2 \in \mathcal{H} = \{h \mid h \text{ is a hyperplane in } \mathbb{R}^d\}$, and $\bar{v}_{Q_i}(h_j)$ is the distance from point q_i in $Q \subset \mathbb{R}^d$ to h_j ($j = 1, 2$). Using the similar method, we can show if there is a subset of $2d + 1$ points in Q and any $d + 1$ points in this subset are not on the same hyperplane, then (4) is a metric in \mathcal{H} .

A.1 Matrix Norm Variant

In another variant of d_Q we define $\tilde{v}_{Q_i}(\ell)$ as a vector from q_i to the closest point on ℓ . More specifically, suppose ℓ is in the same form as before, then the projection of point $q_i = (x_i, y_i)$ on ℓ is $(\tilde{x}_i, \tilde{y}_i) = (x_i \cos^2(\alpha) - y_i \sin(\alpha) \cos(\alpha) - c \sin(\alpha), -x_i \cos(\alpha) \sin(\alpha) + y_i \sin^2(\alpha) - c \cos(\alpha))$, and we define $\tilde{v}_{Q_i}(\ell) = (\tilde{x}_i - x_i, \tilde{y}_i - y_i)$ for $(x_i, y_i) \in Q$, and an $n \times 2$ matrix $V_{Q, \ell} = [\tilde{v}_{Q_1}(\ell); \dots; \tilde{v}_{Q_n}(\ell)]$ where $\tilde{v}_{Q_i}(\ell)$ is the i th row of $V_{Q, \ell}$. For $\ell_1, \ell_2 \in \mathcal{L}$ we define the distance between these two lines as

$$\bar{d}_Q(\ell_1, \ell_2) := \|V_{Q, \ell_1} - V_{Q, \ell_2}\|_F, \quad (5)$$

where $\|\cdot\|_F$ is the Frobenius norm of matrices. For (5), we have the following theorem.

THEOREM A.2. *Suppose in $Q \subset \mathbb{R}^2$ there are two different points q_1 and q_2 , then \bar{d}_Q is a metric in \mathcal{L} .*

PROOF. We only need to show if $\bar{d}_Q(\ell_1, \ell_2) = 0$, then $\ell_1 = \ell_2$. There are two cases.

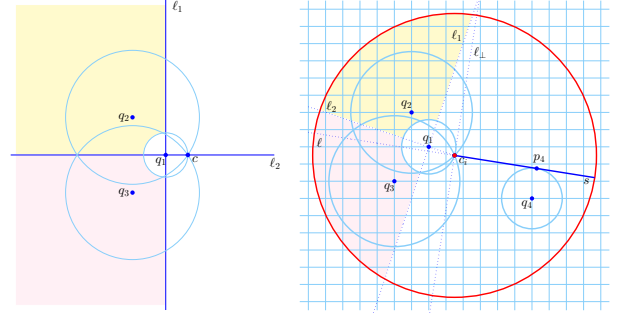


Figure 6: Left: $\ell_1 \perp \ell_2$ and $B(q_1, \|q_1 - c\|) \subset B(q_2, \|q_2 - c\|) \cup B(q_3, \|q_3 - c\|)$. Right: c_i is a critical point of $\gamma^{(1)}$ and $B(q_1, \|q_1 - c_i\|) \subset B(q_2, \|q_2 - c_i\|) \cup B(q_3, \|q_3 - c_i\|)$.

(1) $\tilde{v}_{Q_1}(\ell_1) = (0, 0)$ and $\tilde{v}_{Q_2}(\ell_1) = (0, 0)$. From $\bar{d}_Q(\ell_1, \ell_2) = 0$ we know $\tilde{v}_{Q_1}(\ell_2) = 0$ and $\tilde{v}_{Q_2}(\ell_2) = 0$, which means q_1 and q_2 are on both ℓ_1 and ℓ_2 , so $\ell_1 = \ell_2$.

(2) $\tilde{v}_{Q_1}(\ell_1) \neq (0, 0)$ or $\tilde{v}_{Q_2}(\ell_1) \neq (0, 0)$. In this case, without loss of generality we assume $\tilde{v}_{Q_1}(\ell_1) \neq (0, 0)$. From $\bar{d}_Q(\ell_1, \ell_2) = 0$ we have $\tilde{v}_{Q_1}(\ell_2) = \tilde{v}_{Q_1}(\ell_1) \neq (0, 0)$, so introducing the notation $(\tilde{x}_i - x_i, \tilde{y}_i - y_i) = \tilde{v}_{Q_i}(\ell_1)$, we know $(\tilde{x}_i, \tilde{y}_i)$ is on ℓ_1 and ℓ_2 , and $\tilde{v}_{Q_1}(\ell_1)$ is the normal direction of ℓ_1 and ℓ_2 . Since a point and a normal direction can uniquely determine a line, we have $\ell_1 = \ell_2$. \square

Remark. Definition (5) can be generalized to hyperplanes in \mathbb{R}^d :

$$\bar{d}_Q(h_1, h_2) := \|V_{Q, h_1} - V_{Q, h_2}\|_F, \quad (6)$$

where $h_1, h_2 \in \mathcal{H} = \{h \mid h \text{ is a hyperplane in } \mathbb{R}^d\}$, and V_{Q, h_j} ($j = 1, 2$) is an $n \times d$ matrix with each row being a projection vector from a point in Q to h_j . Using the similar method, we can show if there are d different points in Q , then (6) is a metric in \mathcal{H} .

B Metric Properties for d_Q on Trajectories

In this section, we prove Theorem 3.1 for d_Q . We first introduce the following lemma.

LEMMA B.1. *As shown in Figure 6, suppose the line ℓ_2 passes through q_1 and c , ℓ_1 is perpendicular to ℓ_2 at q_1 , and c is on the right side of ℓ_1 . If q_2 is outside the circle $C(q_1, \|q_1 - c\|)$, on the left side of ℓ_2 and above ℓ_2 (the yellow-shaded region), and q_3 is outside the circle $C(q_1, \|q_1 - c\|)$, on the left side of ℓ_2 and below ℓ_2 (the pink-shaded region), then we have $B(q_1, \|q_1 - c\|) \subset B(q_2, \|q_2 - c\|) \cup B(q_3, \|q_3 - c\|)$.*

PROOF. We use q_1 as the origin, ℓ_2 as the x -axis and ℓ_1 as the y -axis to build a coordinate system, and assume the coordinates of c, q_2 and q_3 are $(r, 0)$, (x_2, y_2) and (x_3, y_3) respectively. So, we have $x_2^2 + y_2^2 > r^2$, $x_3^2 + y_3^2 > r^2$ and $x_2, x_3 < 0$, $y_2 > 0$ and $y_3 < 0$. Our goal is to prove if $x^2 + y^2 \leq r^2$ then either

$$(x - x_2)^2 + (y - y_2)^2 \leq (x_2 - r)^2 + y_2^2, \quad (7)$$

or

$$(x - x_3)^2 + (y - y_3)^2 \leq (x_3 - r)^2 + y_3^2. \quad (8)$$

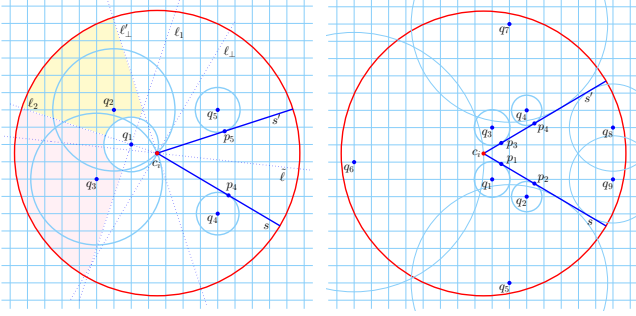


Figure 7: Left: c_i is a critical point of $\gamma^{(1)}$ and $B(q_1, \|q_1 - c_i\|) \subset B(q_2, \|q_2 - c_i\|) \cup B(q_3, \|q_3 - c_i\|)$. **Right:** $B(q_1, \|q_1 - p_1\|)$, $B(q_2, \|q_2 - p_2\|)$ are tangent to s , and $B(q_3, \|q_3 - p_3\|)$, $B(q_4, \|q_4 - p_4\|)$ are tangent to s' . For each one of these four circles, any tangent line segment, except s, s' cannot be extended outside $B(c_i, \frac{\tau}{2})$ without intersecting with any other circle.

If $y \geq 0$, then from $x \leq r, x_2 < 0, y_2 > 0$ we have $(r-x)x_2 \leq yy_2$, which is equivalent to $-2xx_2 - 2yy_2 \leq -2rx_2$. Since $x^2 + y^2 \leq r^2$, we obtain $x^2 - 2xx_2 + y^2 - 2yy_2 \leq -2rx_2 + r^2$, which implies (7) is true. Similarly, if $y \leq 0$ then we can show (8) is true. Thus, the proof is completed. \square

Now, we can give the proof of Theorem 3.1 for d_Q .

PROOF. Suppose $d_Q(\gamma^{(1)}, \gamma^{(2)}) = 0$, we only need to prove $\gamma^{(1)} = \gamma^{(2)}$. We draw a ball $B(c_i, \frac{1}{2}\tau)$ at a critical point c_i ($1 \leq i \leq k-1$) of $\gamma^{(1)}$. There are three possibilities.

Case 1. As shown in Figure 6(Right), c_i is an endpoint of $\gamma^{(1)}$, and $B(c_i, \frac{\tau}{2})$ contains one line segment s of $\gamma^{(1)}$. In this case, we assume s is part of line ℓ , and draw a line ℓ_\perp through c_i which is perpendicular to ℓ . Then, we choose a point q_1 from $Q \cap B(c_i, \frac{\tau}{2})$, which is on the left side of ℓ_\perp , close to ℓ and satisfies $\|q_1 - c\| < 2\eta$. Suppose ℓ_2 is the line through q_1 and c_i , and ℓ_1 is perpendicular to ℓ_2 at q_1 . We choose a point $q_2 \in Q \cap B(c_i, \frac{\tau}{2})$ from the region that is outside $B(q_1, \|q_1 - c_i\|)$, on the left side of ℓ_1 and ℓ_\perp , and above ℓ_2 (the yellow-shaded region), and choose a point $q_3 \in Q \cap B(c_i, \frac{\tau}{2})$ from the region that is outside $B(q_1, \|q_1 - c_i\|)$, on the left side of ℓ_1 and ℓ_\perp , and below ℓ_2 (the pink-shaded region). Obviously, $\{c_i\} = C(q_1, \|q_1 - c_i\|) \cap C(q_2, \|q_2 - c_i\|) \cap C(q_3, \|q_3 - c_i\|)$, and from Lemma B.1, we know $B(q_1, \|q_1 - c_i\|) \subset B(q_2, \|q_2 - c_i\|) \cup B(q_3, \|q_3 - c_i\|)$. So, c_i must be on $\gamma^{(2)}$. Since the tangent line of $C(q_1, \|q_1 - c_i\|)$ at c_i goes into the interior of $B(q_2, \|q_2 - c_i\|)$ and $B(q_3, \|q_3 - c_i\|)$, from (O1) we know c_i must be a critical point of $\gamma^{(2)}$. There also exists $q_4 \in B(c_i, \frac{\tau}{2})$ and $p_4 \in s$ such that $B(q_4, \|q_4 - p_4\|)$ is tangent to s at point p_4 . From (O1) and (O2) we know the tangent line segment of $C(q_4, \|q_4 - p_4\|)$ through c_i must be a part of $\gamma^{(2)}$, and this tangent line segment must be s because the other tangent line segment through c_i intersects with other circles. Thus, s is a part of $\gamma^{(2)}$.

Case 2. As shown in Figure 7(Left), c_i is an internal of $\gamma^{(1)}$, $B(c_i, \frac{\tau}{2})$ contains two line segments s, s' of $\gamma^{(1)}$, and the angle between s, s' is at most $\frac{\pi}{4}$. In this case, we assume $\tilde{\ell}$ is the line bisecting the angle formed by s and s' , and draw two lines ℓ_\perp and

ℓ'_\perp which is perpendicular to s and s' at c_i respectively. Then, we choose a point q_1 from $Q \cap B(c_i, \frac{\tau}{2})$, which is on the left side of ℓ_\perp and ℓ'_\perp , close to $\tilde{\ell}$ and satisfies $\|q_1 - c\| < 2\eta$. Suppose ℓ_2 is the line through q_1 and c_i , and ℓ_1 is perpendicular to ℓ_2 at q_1 . We choose a point $q_2 \in Q \cap B(c_i, \frac{\tau}{2})$ from the region that is outside $B(q_1, \|q_1 - c_i\|)$, on the left side of ℓ_1, ℓ_\perp and ℓ'_\perp and above ℓ_2 (the yellow-shaded region), and choose a point $q_3 \in Q \cap B(c_i, \frac{\tau}{2})$ from the region that is outside $B(q_1, \|q_1 - c_i\|)$, on the left side of ℓ_1, ℓ_\perp and ℓ'_\perp and below ℓ_2 (the pink-shaded region). Obviously, $\{c_i\} = C(q_1, \|q_1 - c_i\|) \cap C(q_2, \|q_2 - c_i\|) \cap C(q_3, \|q_3 - c_i\|)$, and from Lemma B.1, we know $B(q_1, \|q_1 - c_i\|) \subset B(q_2, \|q_2 - c_i\|) \cup B(q_3, \|q_3 - c_i\|)$. So, c_i must be on $\gamma^{(2)}$. Since the tangent line of $C(q_1, \|q_1 - c_i\|)$ at c_i goes into the interior of $B(q_2, \|q_2 - c_i\|)$ and $B(q_3, \|q_3 - c_i\|)$, from (O1) we know c_i must be a critical point of $\gamma^{(2)}$. There also exists $q_4, q_5 \in B(c_i, \frac{\tau}{2})$ and $p_4 \in s, p_5 \in s'$ such that $B(q_4, \|q_4 - p_4\|)$ is tangent to s at point p_4 , and $B(q_5, \|q_5 - p_5\|)$ is tangent to s' at point p_5 . Using the similar argument in Case 1, we can show s and s' both belong to $\gamma^{(2)}$.

Case 3. As shown in Figure 7(Right), c_i is an internal of $\gamma^{(1)}$, $B(c_i, \frac{\tau}{2})$ contains two line segments s, s' of $\gamma^{(1)}$, and the angle between s, s' is greater than $\frac{\pi}{4}$. In this case, we choose four points q_1, q_2, q_3, q_4 from $Q \cap B(c_i, \frac{\tau}{2})$ such that the circles with center q_1, q_2 are tangent to s at p_1, p_2 , and the circles with center q_3, q_4 are tangent to s' at p_3, p_4 . Moreover, we can require $\|q_j - c_j\| \leq \eta$ for $1 \leq j \leq 4$ and these four circles do not intersect with each other. Then, we can choose three points q_5, q_6, q_7 outside the angle region formed by s and s' , and two points q_8, q_9 inside this angle region. Using $C_{j'}$ ($5 \leq j' \leq 9$) to represent the circles corresponding to these five points, we can choose these points close to the boundary of $B(c_i, \frac{\tau}{2})$, and require C_6 contains c_i , C_5, C_9 are tangent to s , C_7, C_8 are tangent to s' , and $C_5 \cap C_6 \neq \emptyset, C_6 \cap C_7 \neq \emptyset$, and $C_8 \cap C_9 \neq \emptyset$. Thus, any tangent line segment of $C(q_j, \|q_j - p_j\|)$ ($1 \leq j \leq 4$), except s, s' , can not be extended outside $B(c_i, \frac{\tau}{2})$ without intersecting with $\cup_{5 \leq j' \leq 9} C_{j'}$. From (O1) and (O2) we know $\gamma^{(2)}$ must be tangent to $C(q_1, \|q_1 - p_1\|)$ or $C(q_2, \|q_2 - p_2\|)$, and without loss of generality we assume a tangent line segment of $C(q_1, \|q_1 - p_1\|)$ is a part of $\gamma^{(2)}$. Since (O2), (O3) imply this tangent line segment must be extended outside $B(c_i, \frac{\tau}{2})$ without going into the interior of any other circle, we know $s \cap B(q_1, \delta)$ is a part of $\gamma^{(2)}$ for some $\delta > 0$. Similarly, we have $s' \cap B(q_3, \delta)$ is a part of $\gamma^{(2)}$ for some $\delta > 0$. Since there is at most one critical point of $\gamma^{(2)}$ in $B(c_i, \frac{\tau}{2})$, from (O3) we know c_i must be a critical point of $\gamma^{(2)}$. Thus, s and s' both belong to $\gamma^{(2)}$. \square

From the discussion of above three cases, we know $\gamma^{(2)}$ overlaps with $\gamma^{(1)}$ in the ball $B(c_i, \frac{\tau}{2})$, and a similar argument leads to $\gamma^{(1)} = \gamma^{(2)}$. \square

C Common Distance Measurements for Trajectories

In this section, we briefly introduce the definition of Euclidian distance, discrete Frechet distance and dynamic time warping distance. Suppose $\gamma^{(1)}$ and $\gamma^{(2)}$ are two trajectories in \mathbb{R}^2 with critical points $c_0^{(1)}, c_1^{(1)}, \dots, c_{k_1}^{(1)}$ and $c_0^{(2)}, c_1^{(2)}, \dots, c_{k_2}^{(2)}$ respectively.

Euclidean Distance. It requires $k_1 = k_2$ and takes the average Euclidean distance between corresponding critical points.

$$\text{Eu}(\gamma^{(1)}, \gamma^{(2)}) = \frac{1}{k_1} \sum_{i=0}^{k_1} \|c_i^{(1)} - c_i^{(2)}\|.$$

Discrete Frechet Distance. It measures the similarity between two piecewise-linear curves by taking into account their location and time ordering. Here, we introduce its definition in [6]. Suppose $\mathcal{A} = \{a_0, a_1, \dots, a_m\} \subset \{0, 1, \dots, k_1\}$, $\mathcal{B} = \{b_0, b_1, \dots, b_m\} \subset \{0, 1, \dots, k_2\}$, and $a_0 = b_0 = 0$, $a_m = k_1$, $b_m = k_2$. If for each $i \in \{0, \dots, k_1 - 1\}$ we have $a_{i+1} = a_i$ or $a_{i+1} = a_i + 1$, and for each $i \in \{0, \dots, k_2 - 1\}$, we have $b_{i+1} = b_i$ or $b_{i+1} = b_i + 1$, then we say \mathcal{A} and \mathcal{B} can determine a coupling \mathcal{L} between $\gamma^{(1)}$ and $\gamma^{(2)}$, which is a sequence $(c_{a_0}^{(1)}, c_{b_0}^{(2)}), (c_{a_1}^{(1)}, c_{b_1}^{(2)}), \dots, (c_{a_m}^{(1)}, c_{b_m}^{(2)})$. We define the length of \mathcal{L} as $\|\mathcal{L}\| = \max_{0 \leq i \leq m} \|c_{a_i}^{(1)} - c_{b_i}^{(2)}\|$. The discrete Frechet distance is defined as:

$$\begin{aligned} \text{dF}(\gamma^{(1)}, \gamma^{(2)}) \\ = \min\{\|\mathcal{L}\| \mid \mathcal{L} \text{ is a coupling between } \gamma^{(1)} \text{ and } \gamma^{(2)}\}. \end{aligned}$$

Dynamic Time Warping (DTW) Distance. DTW [24] is an algorithm to find the optimal matching between the critical points of two trajectories, and it does not require $k_1 = k_2$. It is defined and computed by the recursion formula: $D(i, j) = \|c_i^{(1)} - c_j^{(2)}\| + \min(D(i-1, j), D(i-1, j-1), D(i, j-1))$, where $D(0, j) = \|c_0^{(1)} - c_j^{(2)}\|$, $D(i, 0) = \|c_i^{(1)} - c_0^{(2)}\|$, and DTW distance between $\gamma^{(1)}$ and $\gamma^{(2)}$ is defined as $\text{DTW}(\gamma^{(1)}, \gamma^{(2)}) = D(k_1, k_2)$.

Discrete Hausdorff Distance. It measure the spatial similarity between two trajectories [16]:

$$\text{dH}(\gamma^{(1)}, \gamma^{(2)}) = \max(d(\gamma^{(1)}, \gamma^{(2)}), d(\gamma^{(2)}, \gamma^{(1)}))$$

where $d(\gamma^{(1)}, \gamma^{(2)}) = \max_{0 \leq i \leq k_1} \min_{0 \leq j \leq k_2} \|c_i^{(1)} - c_j^{(2)}\|$.

Longest Common Subsequence Distance. It finds the alignment between two sequences that maximize the length of common subsequence. Let $\text{Head}(\gamma^{(1)})$ be the first $k_1 - 1$ critical points of $\gamma^{(1)}$, and $\text{Head}(\gamma^{(2)})$ be the first $k_2 - 1$ critical points of $\gamma^{(2)}$. Given $\epsilon, \delta > 0$, the $\text{lcss}_{\epsilon, \delta}(\gamma^{(1)}, \gamma^{(2)})$ is defined as follows [25]:

$$\text{lcss}_{\epsilon, \delta}(\gamma^{(1)}, \gamma^{(2)}) = \begin{cases} 0, & \text{if } \gamma^{(1)} \text{ or } \gamma^{(2)} \text{ is empty} \\ 1 + \text{lcss}_{\epsilon, \delta}(\gamma^{(1)}, \gamma^{(2)}), & \text{if } \|c_{k_1}^{(1)} - c_{k_2}^{(2)}\| < \epsilon \text{ and } |k_1 - k_2| < \delta \\ \max(\text{lcss}_{\epsilon, \delta}(\text{Head}(\gamma^{(1)}), \gamma^{(2)}), \text{lcss}_{\epsilon, \delta}(\gamma^{(1)}, \text{Head}(\gamma^{(2)}))), & \text{otherwise} \end{cases}$$

LCSS distance is defined as $\text{LCSS}_{\epsilon, \delta}(\gamma^{(1)}, \gamma^{(2)}) = 1 - \frac{\text{lcss}_{\epsilon, \delta}(\gamma^{(1)}, \gamma^{(2)})}{\max(k_1, k_2)}$.

Edit Distance for Real Sequences. It is similar to the edit distance on strings, and seeking the minimum number of edit operations required to change one trajectory to another [4]. For EDR with $\epsilon > 0$, $\gamma^{(1)}$ and $\gamma^{(2)}$ are considered to be the same if $k_1 = k_2$ and $\|c_i^{(1)} - c_i^{(2)}\| < \epsilon$.

Locality Sensitive Hashing Distance. Given a point set $Q \subset \mathbb{R}^2$, and $r > 0$, it consider the disks with centers in Q and radius equal to r . For LSH1_Q , each trajectory is converted to a bit vector of length $|Q|$, and each bit represents the intersection of the trajectory with a disk, and uses Hamming distance of two bit vectors to define

the distance between two curves. For LSH2_Q , each trajectories is converted to a sequence representing the order in which the trajectory enters and exits the disks, and uses edit distance of two sequence to define the distance between two curves [3].

D More Trajectory Experiments

D.1 Different Weightings

For SVM with linear kernel and quadratic kernel, as we increase w_1 , the error of d_Q and d_Q^π also decreases, although not as obvious as Gaussian kernel. The results are shown in Table 10 and Table 11.

Table 10: Landmark-sensitive classification error with weighted linear SVM.

metrics	mean	median	variance
$d_{Q, W} (w_1 = 0.3)$	0.3309	0.3333	0.0070
$d_{Q, W} (w_1 = 0.6)$	0.3083	0.3333	0.0104
$d_{Q, W} (w_1 = 0.9)$	0.3051	0.3333	0.0119
$d_{Q, W}^\pi (w_1 = 0.3)$	0.4936	0.5000	0.0082
$d_{Q, W}^\pi (w_1 = 0.6)$	0.4191	0.4444	0.0049
$d_{Q, W}^\pi (w_1 = 0.9)$	0.4104	0.3889	0.0048
$d_{Q, W}^{\leftrightarrow} (w_1 = 0.3)$	0.4372	0.4444	0.0081
$d_{Q, W}^{\leftrightarrow} (w_1 = 0.6)$	0.4340	0.4444	0.0080
$d_{Q, W}^{\leftrightarrow} (w_1 = 0.9)$	0.4329	0.4444	0.0080

Table 11: Landmark-sensitive classification error with weighted quadratic SVM.

metrics	mean	median	variance
$d_{Q, W} (w_1 = 0.3)$	0.3309	0.3333	0.0070
$d_{Q, W} (w_1 = 0.6)$	0.3084	0.3333	0.0104
$d_{Q, W} (w_1 = 0.9)$	0.3051	0.3333	0.0119
$d_{Q, W}^\pi (w_1 = 0.3)$	0.5302	0.5000	0.0098
$d_{Q, W}^\pi (w_1 = 0.6)$	0.5270	0.5000	0.0105
$d_{Q, W}^\pi (w_1 = 0.9)$	0.3909	0.3889	0.0060
$d_{Q, W}^{\leftrightarrow} (w_1 = 0.3)$	0.4367	0.4444	0.0081
$d_{Q, W}^{\leftrightarrow} (w_1 = 0.6)$	0.4333	0.4444	0.0079
$d_{Q, W}^{\leftrightarrow} (w_1 = 0.9)$	0.4322	0.4444	0.0079

D.2 The error of LCSS, EAR and LSH with Other Parameters in Section 4

In the experiment of Section 4, the computation of LCSS, EAR LSH1_Q and LSH2_Q involves some parameters, and we only give the result of best parameter for these distances. In this section, we describe the change of error statics for these distances with different parameters, and show how we obtain the best parameter in each experiment. We use bold font to mark the smallest mean error and the corresponding median and variance.

Table 12: Mean error of LCSS in Table 1 with different parameters.

mean \ ϵ		0.0010	0.0050	0.0100	0.0150	0.0200	0.0250	0.0300	0.0350	0.0400	0.0450	0.0500	0.0550
δ													
1		0.1115	0.0822	0.0856	0.0969	0.1105	0.1297	0.1532	0.1749	0.1902	0.2003	0.2087	0.2182
2		0.0940	0.0785	0.0840	0.0954	0.1085	0.1278	0.1511	0.1731	0.1879	0.1987	0.2064	0.2164
3		0.0901	0.0769	0.0833	0.0946	0.1078	0.1271	0.1503	0.1718	0.1865	0.1977	0.2057	0.2160
4		0.0860	0.0755	0.0823	0.0936	0.1077	0.1267	0.1496	0.1707	0.1861	0.1966	0.2050	0.2151
5		0.0846	0.0745	0.0819	0.0935	0.1079	0.1269	0.1495	0.1704	0.1857	0.1961	0.2046	0.2150
6		0.0826	0.0739	0.0821	0.0939	0.1079	0.1265	0.1494	0.1706	0.1855	0.1958	0.2045	0.2149
7		0.0816	0.0734	0.0823	0.0937	0.1078	0.1261	0.1490	0.1702	0.1853	0.1957	0.2043	0.2147
8		0.0802	0.0729	0.0817	0.0935	0.1075	0.1261	0.1489	0.1702	0.1852	0.1957	0.2041	0.2145
9		0.0795	0.0721	0.0815	0.0933	0.1075	0.1262	0.1490	0.1699	0.1849	0.1955	0.2039	0.2142
10		0.0783	0.0714	0.0811	0.0930	0.1072	0.1258	0.1485	0.1695	0.1845	0.1951	0.2037	0.2140

Table 13: Median error of LCSS in Table 1 with different parameters.

mean \ ϵ		0.0010	0.0050	0.0100	0.0150	0.0200	0.0250	0.0300	0.0350	0.0400	0.0450	0.0500	0.0550
δ													
1		0.0869	0.0577	0.0589	0.0652	0.0741	0.0889	0.1029	0.1143	0.1240	0.1325	0.1387	0.1474
2		0.0707	0.0536	0.0576	0.0643	0.0722	0.0868	0.1000	0.1118	0.1222	0.1304	0.1360	0.1458
3		0.0667	0.0531	0.0571	0.0640	0.0720	0.0867	0.1000	0.1103	0.1200	0.1297	0.1357	0.1464
4		0.0625	0.0526	0.0565	0.0640	0.0720	0.0864	0.1000	0.1094	0.1200	0.1278	0.1353	0.1449
5		0.0608	0.0524	0.0564	0.0643	0.0728	0.0865	0.1000	0.1087	0.1194	0.1274	0.1357	0.1449
6		0.0590	0.0516	0.0567	0.0649	0.0729	0.0857	0.1000	0.1088	0.1189	0.1267	0.1353	0.1449
7		0.0583	0.0512	0.0571	0.0647	0.0728	0.0857	0.0987	0.1088	0.1187	0.1267	0.1353	0.1446
8		0.0571	0.0506	0.0568	0.0646	0.0730	0.0857	0.0984	0.1083	0.1187	0.1266	0.1346	0.1444
9		0.0566	0.0500	0.0564	0.0645	0.0731	0.0857	0.0984	0.1079	0.1182	0.1261	0.1340	0.1444
10		0.0556	0.0500	0.0563	0.0643	0.0728	0.0850	0.0976	0.1076	0.1179	0.1256	0.1336	0.1440

Table 14: Error variance of LCSS in Table 1 with different parameters.

variance \ ϵ		0.0010	0.0050	0.0100	0.0150	0.0200	0.0250	0.0300	0.0350	0.0400	0.0450	0.0500	0.0550
δ													
1		0.0087	0.0070	0.0077	0.0099	0.0127	0.0162	0.0220	0.0280	0.0315	0.0336	0.0350	0.0367
2		0.0073	0.0068	0.0075	0.0096	0.0123	0.0161	0.0218	0.0276	0.0311	0.0335	0.0349	0.0365
3		0.0072	0.0063	0.0074	0.0094	0.0121	0.0160	0.0216	0.0274	0.0310	0.0333	0.0348	0.0364
4		0.0068	0.0060	0.0072	0.0092	0.0121	0.0158	0.0216	0.0273	0.0310	0.0332	0.0346	0.0363
5		0.0068	0.0058	0.0071	0.0091	0.0120	0.0158	0.0215	0.0273	0.0309	0.0332	0.0346	0.0363
6		0.0065	0.0058	0.0071	0.0090	0.0120	0.0158	0.0215	0.0273	0.0309	0.0332	0.0346	0.0363
7		0.0065	0.0057	0.0071	0.0090	0.0120	0.0158	0.0214	0.0272	0.0308	0.0331	0.0346	0.0363
8		0.0063	0.0056	0.0070	0.0090	0.0120	0.0158	0.0215	0.0272	0.0308	0.0331	0.0346	0.0363
9		0.0063	0.0056	0.0070	0.0090	0.0120	0.0158	0.0215	0.0273	0.0308	0.0332	0.0346	0.0363
10		0.0060	0.0054	0.0070	0.0089	0.0119	0.0157	0.0214	0.0272	0.0308	0.0332	0.0346	0.0363

Table 15: Classification Error of EDR in Table 1 with different parameters.

ϵ	0.0010	0.0050	0.0100	0.0150	0.0200	0.0250	0.0300	0.0350	0.0400	0.0450	0.0500	0.0550
mean	0.1070	0.0802	0.0846	0.0957	0.1096	0.1289	0.1521	0.1744	0.1894	0.1997	0.2078	0.2175
median	0.0833	0.0554	0.0581	0.0640	0.0731	0.0875	0.1009	0.1139	0.1229	0.1319	0.1378	0.1462
variance	0.0084	0.0070	0.0077	0.0098	0.0127	0.0162	0.0219	0.0279	0.0314	0.0336	0.0350	0.0367

Table 16: Classification Error of LSH1_Q and LSH2_Q in Table 1 with different parameters.

r		0.0050	0.0100	0.0200	0.0300	0.0400	0.0500	0.0600	0.0700	0.0800	0.0900	0.1000	0.1100
LSH1 _Q	mean	0.4145	0.3792	0.3143	0.2645	0.2197	0.1374	0.1290	0.1501	0.1487	0.1774	0.1680	0.1633
	median	0.3913	0.3500	0.2693	0.2121	0.1667	0.1000	0.0949	0.1114	0.1046	0.1133	0.1154	0.1179
	variance	0.0616	0.0530	0.0448	0.0404	0.0315	0.0153	0.0128	0.0168	0.0176	0.0286	0.0232	0.0207
LSH2 _Q	mean	0.4161	0.3873	0.3449	0.3043	0.2798	0.2637	0.2574	0.2494	0.2445	0.2415	0.2409	0.2426
	median	0.3919	0.3644	0.3154	0.2605	0.2333	0.2281	0.2255	0.2275	0.2216	0.2195	0.2182	0.2191
	variance	0.0621	0.0531	0.0457	0.0405	0.0381	0.0301	0.0271	0.0224	0.0220	0.0210	0.0210	0.0215

Table 17: Mean error of LCSS in Table 4 with different parameters.

mean ϵ		δ											
δ		0.0010	0.0050	0.0100	0.0150	0.0200	0.0250	0.0300	0.0350	0.0400	0.0450	0.0500	0.0550
1	1	0.2761	0.2956	0.2634	0.2676	0.2839	0.3046	0.3049	0.3147	0.3256	0.3459	0.3527	0.3582
2	1	0.3123	0.2761	0.2718	0.2647	0.2866	0.3148	0.3112	0.3160	0.3267	0.3458	0.3552	0.3598
3	1	0.3116	0.2905	0.2685	0.2448	0.2941	0.3350	0.3129	0.3160	0.3267	0.3458	0.3542	0.3598
4	1	0.3112	0.2911	0.2552	0.2556	0.2937	0.3347	0.3135	0.3160	0.3267	0.3458	0.3542	0.3598
5	1	0.2823	0.2919	0.2680	0.2656	0.2965	0.3352	0.3135	0.3160	0.3267	0.3458	0.3542	0.3598
6	1	0.2883	0.2904	0.2691	0.2726	0.2965	0.3352	0.3135	0.3160	0.3267	0.3458	0.3542	0.3596
7	1	0.2931	0.2887	0.2645	0.2726	0.2965	0.3352	0.3135	0.3160	0.3267	0.3458	0.3542	0.3598
8	1	0.2952	0.2828	0.2655	0.2726	0.2965	0.3352	0.3135	0.3160	0.3267	0.3458	0.3542	0.3598
19	1	0.2946	0.2831	0.2655	0.2726	0.2965	0.3352	0.3135	0.3160	0.3267	0.3458	0.3542	0.3598
10	1	0.2934	0.2831	0.2655	0.2726	0.2965	0.3352	0.3135	0.3160	0.3267	0.3458	0.3542	0.3598

Table 18: Median error of LCSS in Table 4 with different parameters.

median ϵ		δ											
δ		0.0010	0.0050	0.0100	0.0150	0.0200	0.0250	0.0300	0.0350	0.0400	0.0450	0.0500	0.0550
1	1	0.2778	0.3056	0.2500	0.2778	0.2778	0.3056	0.3056	0.3056	0.3333	0.3611	0.3611	0.3611
2	1	0.3056	0.2778	0.2778	0.2500	0.2778	0.3056	0.3056	0.3056	0.3333	0.3611	0.3611	0.3611
3	1	0.3056	0.2778	0.2778	0.2500	0.2778	0.3333	0.3056	0.3056	0.3333	0.3611	0.3611	0.3611
4	1	0.3056	0.2778	0.2500	0.2500	0.2778	0.3333	0.3056	0.3056	0.3333	0.3611	0.3611	0.3611
5	1	0.2778	0.2778	0.2778	0.2500	0.3056	0.3333	0.3056	0.3056	0.3333	0.3611	0.3611	0.3611
6	1	0.2778	0.2778	0.2778	0.2778	0.3056	0.3333	0.3056	0.3056	0.3333	0.3611	0.3611	0.3611
7	1	0.3056	0.2778	0.2500	0.2778	0.3056	0.3333	0.3056	0.3056	0.3333	0.3611	0.3611	0.3611
8	1	0.3056	0.2778	0.2500	0.2778	0.3056	0.3333	0.3056	0.3056	0.3333	0.3611	0.3611	0.3611
9	1	0.3056	0.2778	0.2500	0.2778	0.3056	0.3333	0.3056	0.3056	0.3333	0.3611	0.3611	0.3611
10	1	0.3056	0.2778	0.2500	0.2778	0.3056	0.3333	0.3056	0.3056	0.3333	0.3611	0.3611	0.3611

Table 19: Error variance of LCSS in Table 4 with different parameters.

variance ϵ		δ											
δ		0.0010	0.0050	0.0100	0.0150	0.0200	0.0250	0.0300	0.0350	0.0400	0.0450	0.0500	0.0550
1	1	0.0030	0.0037	0.0038	0.0041	0.0036	0.0034	0.0025	0.0013	0.0008	0.0004	0.0002	0.0003
2	1	0.0034	0.0035	0.0038	0.0038	0.0036	0.0038	0.0026	0.0012	0.0007	0.0003	0.0002	0.0003
3	1	0.0030	0.0035	0.0038	0.0037	0.0037	0.0038	0.0025	0.0012	0.0007	0.0003	0.0002	0.0003
4	1	0.0030	0.0036	0.0035	0.0037	0.0036	0.0038	0.0025	0.0012	0.0007	0.0003	0.0002	0.0003
5	1	0.0031	0.0035	0.0037	0.0039	0.0035	0.0038	0.0025	0.0012	0.0007	0.0003	0.0002	0.0003
6	1	0.0029	0.0033	0.0036	0.0039	0.0035	0.0038	0.0025	0.0012	0.0007	0.0003	0.0002	0.0003
7	1	0.0029	0.0034	0.0035	0.0040	0.0035	0.0038	0.0025	0.0012	0.0007	0.0003	0.0002	0.0003
8	1	0.0030	0.0031	0.0035	0.0040	0.0035	0.0038	0.0025	0.0012	0.0007	0.0003	0.0002	0.0003
9	1	0.0029	0.0031	0.0035	0.0040	0.0035	0.0038	0.0025	0.0012	0.0007	0.0003	0.0002	0.0003
10	1	0.0029	0.0031	0.0035	0.0040	0.0035	0.0038	0.0025	0.0012	0.0007	0.0003	0.0002	0.0003

Table 20: Classification error of EDR in Table 4 with different parameters.

ϵ	0.0010	0.0050	0.0100	0.0150	0.0200	0.0250	0.0300	0.0350	0.0400	0.0450	0.0500	0.0550
mean	0.2748	0.2932	0.2661	0.2640	0.2854	0.3036	0.3050	0.3147	0.3256	0.3459	0.3527	0.3582
median	0.2778	0.2778	0.2639	0.2500	0.2778	0.3056	0.3056	0.3056	0.3333	0.3611	0.3611	0.3611
variance	0.0028	0.0038	0.0037	0.0039	0.0035	0.0035	0.0025	0.0013	0.0008	0.0004	0.0002	0.0003

Table 21: Classification error of LSH1_Q and LSH2_Q in Table 4 with different parameters.

r	0.0050	0.0100	0.0200	0.0300	0.0400	0.0500	0.0600	0.0700	0.0800	0.0900	0.1000	0.1100
LSH1 _{Q₁}	mean	0.3360	0.2767	0.2673	0.2784	0.3211	0.3804	0.3647	0.3707	0.3627	0.3616	0.3659
	median	0.3611	0.2778	0.2778	0.2778	0.3333	0.3611	0.3611	0.3611	0.3611	0.3611	0.3611
	variance	0.0013	0.0026	0.0020	0.0028	0.0038	0.0012	0.0007	0.0012	0.0002	0.0000	0.0000
LSH2 _{Q₁}	mean	0.3361	0.2959	0.2789	0.2997	0.2869	0.2830	0.2811	0.2543	0.2516	0.2619	0.2684
	median	0.3611	0.3056	0.2778	0.3056	0.2778	0.2778	0.2778	0.2500	0.2500	0.2778	0.2778
	variance	0.0013	0.0020	0.0016	0.0026	0.0027	0.0031	0.0022	0.0021	0.0022	0.0017	0.0016
LSH1 _{Q₂}	mean	0.3365	0.2517	0.2352	0.2209	0.2468	0.2642	0.3334	0.3020	0.3754	0.3668	0.3626
	median	0.3333	0.2500	0.2222	0.2222	0.2500	0.2500	0.3333	0.3056	0.3611	0.3611	0.3611
	variance	0.0007	0.0026	0.0037	0.0039	0.0035	0.0027	0.0028	0.0024	0.0009	0.0005	0.0004
LSH2 _{Q₂}	mean	0.3472	0.3480	0.3428	0.2879	0.3131	0.2690	0.2945	0.2857	0.3217	0.3072	0.3249
	median	0.3611	0.3611	0.3333	0.2778	0.3056	0.2778	0.3056	0.2778	0.3333	0.3056	0.3333
	variance	0.0008	0.0006	0.0022	0.0018	0.0028	0.0022	0.0023	0.0023	0.0015	0.0021	0.0022

Table 22: Mean error of LCSS in Table 5 with different parameters.

mean ϵ	δ	0.0010	0.0050	0.0100	0.0150	0.0200	0.0250	0.0300	0.0350	0.0400	0.0450	0.0500	0.0550
1	1	0.4961	0.4776	0.4484	0.4584	0.4068	0.4395	0.4412	0.4033	0.4233	0.4585	0.5073	0.5142
2	2	0.4112	0.3867	0.4405	0.4520	0.4363	0.4539	0.4238	0.4611	0.4999	0.5007	0.5062	0.5299
3	3	0.4025	0.4163	0.4903	0.4728	0.4343	0.4307	0.4389	0.4448	0.4656	0.4737	0.4814	0.5158
4	4	0.3504	0.4115	0.4320	0.4481	0.4435	0.4066	0.4319	0.4546	0.4397	0.4511	0.4631	0.4901
5	5	0.3509	0.4190	0.4082	0.4217	0.4177	0.4061	0.4378	0.4453	0.4606	0.4389	0.4738	0.4983
6	6	0.3481	0.4117	0.3961	0.4000	0.3939	0.4045	0.4368	0.4465	0.4592	0.4391	0.4759	0.4993
7	7	0.3527	0.4241	0.3996	0.4009	0.3947	0.4071	0.4308	0.4387	0.4569	0.4397	0.4780	0.4993
8	8	0.3437	0.4141	0.3998	0.4009	0.3947	0.4064	0.4308	0.4324	0.4554	0.4390	0.4780	0.4993
9	9	0.3499	0.4244	0.4039	0.3969	0.3961	0.4064	0.4308	0.4324	0.4554	0.4390	0.4780	0.4993
10	10	0.3582	0.4329	0.4041	0.3969	0.3961	0.4064	0.4308	0.4324	0.4554	0.4390	0.4780	0.4993

Table 23: Median error of LCSS in Table 5 with different parameters.

median ϵ	δ	0.0010	0.0050	0.0100	0.0150	0.0200	0.0250	0.0300	0.0350	0.0400	0.0450	0.0500	0.0550
1	1	0.5000	0.5000	0.4444	0.4444	0.3889	0.4444	0.4444	0.3889	0.4444	0.4444	0.5000	0.5000
2	2	0.3889	0.3889	0.4444	0.4444	0.4444	0.4444	0.4444	0.4444	0.5000	0.5000	0.5000	0.5000
3	3	0.3889	0.4444	0.5000	0.4444	0.4444	0.4444	0.4444	0.4444	0.4444	0.4444	0.5000	0.5000
4	4	0.3333	0.3889	0.4444	0.4444	0.4444	0.3889	0.4444	0.4444	0.4444	0.4444	0.4444	0.5000
5	5	0.3333	0.4444	0.3889	0.4444	0.4444	0.3889	0.4444	0.4444	0.4444	0.4444	0.5000	0.5000
6	6	0.3333	0.3889	0.3889	0.3889	0.3889	0.3889	0.4444	0.4444	0.4444	0.4444	0.5000	0.5000
7	7	0.3333	0.4444	0.3889	0.3889	0.3889	0.3889	0.4444	0.4444	0.4444	0.4444	0.5000	0.5000
8	8	0.3333	0.4167	0.3889	0.3889	0.3889	0.3889	0.4444	0.4444	0.4444	0.4444	0.5000	0.5000
9	9	0.3333	0.4444	0.3889	0.3889	0.3889	0.3889	0.4444	0.4444	0.4444	0.4444	0.5000	0.5000
10	10	0.3333	0.4444	0.3889	0.3889	0.3889	0.3889	0.4444	0.4444	0.4444	0.4444	0.5000	0.5000

Table 24: Error variance of LCSS in Table 5 with different parameters.

variance \ δ \ ϵ	0.0010	0.0050	0.0100	0.0150	0.0200	0.0250	0.0300	0.0350	0.0400	0.0450	0.0500	0.0550
1	0.0015	0.0036	0.0064	0.0062	0.0070	0.0068	0.0066	0.0058	0.0061	0.0068	0.0076	0.0077
2	0.0051	0.0063	0.0066	0.0070	0.0074	0.0062	0.0069	0.0069	0.0069	0.0073	0.0074	0.0081
3	0.0053	0.0058	0.0071	0.0070	0.0068	0.0056	0.0069	0.0069	0.0079	0.0084	0.0079	0.0093
4	0.0058	0.0065	0.0073	0.0072	0.0073	0.0058	0.0074	0.0072	0.0078	0.0080	0.0077	0.0090
5	0.0069	0.0078	0.0077	0.0073	0.0063	0.0059	0.0072	0.0072	0.0076	0.0078	0.0078	0.0091
6	0.0070	0.0075	0.0077	0.0075	0.0067	0.0059	0.0074	0.0070	0.0072	0.0078	0.0077	0.0090
7	0.0066	0.0072	0.0076	0.0079	0.0070	0.0058	0.0072	0.0068	0.0070	0.0078	0.0076	0.0090
8	0.0066	0.0074	0.0076	0.0079	0.0070	0.0057	0.0072	0.0063	0.0069	0.0077	0.0076	0.0090
9	0.0066	0.0072	0.0076	0.0078	0.0068	0.0057	0.0072	0.0063	0.0069	0.0077	0.0076	0.0090
10	0.0066	0.0070	0.0076	0.0078	0.0068	0.0057	0.0072	0.0063	0.0069	0.0077	0.0076	0.0090

Table 25: Classification error of EDR in Table 5 with different parameters.

ϵ	0.0010	0.0050	0.0100	0.0150	0.0200	0.0250	0.0300	0.0350	0.0400	0.0450	0.0500	0.0550
mean	0.4632	0.4541	0.4171	0.4450	0.3916	0.4134	0.4422	0.4259	0.4618	0.4559	0.4681	0.5123
median	0.4444	0.4444	0.4444	0.4444	0.3889	0.3889	0.4444	0.4444	0.4444	0.4444	0.4444	0.5000
variance	0.0026	0.0043	0.0065	0.0068	0.0068	0.0064	0.0058	0.0060	0.0062	0.0079	0.0081	0.0087

Table 26: Classification Error of LSH1_Q and LSH2_Q in Table 5 with different parameters.

r	0.0050	0.0100	0.0200	0.0300	0.0400	0.0500	0.0600	0.0700	0.0800	0.0900	0.1000	0.1100	
LSH1 _Q	mean	0.5098	0.2524	0.2950	0.4878	0.4443	0.4691	0.4494	0.4558	0.5046	0.5103	0.4439	0.4305
	median	0.5000	0.2222	0.2778	0.5000	0.4444	0.4444	0.4444	0.4444	0.5000	0.5000	0.4444	0.4444
	variance	0.0006	0.0098	0.0067	0.0064	0.0062	0.0066	0.0085	0.0059	0.0045	0.0068	0.0068	0.0061
LSH2 _Q	mean	0.5000	0.4547	0.3248	0.3850	0.5271	0.5400	0.5216	0.5130	0.4828	0.4943	0.4406	0.4865
	median	0.5000	0.4444	0.3333	0.3889	0.5278	0.5556	0.5000	0.5000	0.5000	0.5000	0.4444	0.5000
	variance	0	0.0074	0.0084	0.0076	0.0068	0.0049	0.0046	0.0072	0.0052	0.0049	0.0076	0.0070